Column-Compound Extremes in the Global Ocean

Joel Wong[1], Matthias Münnich[1], and Nicolas Gruber[1]

[1]ETH Zürich

October 17, 2023

Abstract

Marine extreme events such as marine heatwaves, ocean acidity extremes and low oxygen extremes can pose a substantial threat to marine organisms and ecosystems. Such extremes might be particularly detrimental (i) when they occur compounded in more than one stressor, and (ii) when the extremes extend substantially across the water column, restricting the habitable space for marine organisms. Here, we use daily output from a hindcast simulation (1961-2020) from the ocean component of the Community Earth System Model (CESM) to characterise such column-compound extreme events (CCX), employing a relative threshold approach to identify the extremes and requiring them to extend vertically over at least 50m. The diagnosed CCXs are prevalent, occupying worldwide in the 1960s about 1% of the volume contained within the top 300m. Over the duration of our simulation, CCXs become more intense, last longer, and occupy more volume, driven by the trends in ocean warming and ocean acidification. For example, the triple CCX have expanded 24-fold, now last 3-times longer, and have become 6-times more intense since the early 1960s. Removing this effect with a moving baseline permits us to better understand the key characteristics of the CCXs. They last typically about 10 to 30 days and predominantly occur in the tropics and the high latitudes, regions of high potential biological vulnerability. Overall, the CCXs fall into 16 clusters, reflecting different patterns and drivers. Triple CCX are largely confined to the tropics and the North Pacific, and tend to be associated with the El Nino-Southern Oscillation.

Column-Compound Extremes in the Global Ocean

Joel Wong[1], Matthias Münnich[1], and Nicolas Gruber[1]

[1]Environmental Physics, Institute of Biogeochemistry and Pollutant Dynamics, ETH Zurich, Zürich, Switzerland

Key Points:

- Column-compound extremes (CCX): defined when 50 m of the top 300 m is extreme in multiple parameters, reduce habitable space by up to 75%.
- From 1961 to 2020, CCX have become more intense, longer, and occupy more volume, driven by the trends in ocean warming and acidification.
- Triple CCX are largely confined to the tropics and the North Pacific, have high intensity, and severely reduces habitable space.

Corresponding author: Joel Wong, `joel.wong@usys.ethz.ch`

Abstract

Marine extreme events such as marine heatwaves, ocean acidity extremes and low oxygen extremes can pose a substantial threat to marine organisms and ecosystems. Such extremes might be particularly detrimental (i) when they occur compounded in more than one stressor, and (ii) when the extremes extend substantially across the water column, restricting the habitable space for marine organisms. Here, we use daily output of a hindcast simulation (1961-2020) from the ocean component of the Community Earth System Model to characterise such column-compound extreme events (CCX), employing a relative threshold approach to identify extremes and requiring them to extend vertically over at least 50 m. The diagnosed CCXs are prevalent, occupying worldwide in the 1960s about 1% of the volume contained within the top 300 m. Over the duration of our simulation, CCXs become more intense, last longer, and occupy more volume, driven by the trends in ocean warming and ocean acidification. For example, the triple CCX expanded 24-fold, now last 3-times longer, and became 6-times more intense since the early 1960s. Removing this effect with a moving baseline permits us to better understand the key characteristics of the CCXs. They last typically about 10 to 30 days and predominantly occur in the tropics and the high latitudes, regions of high potential biological vulnerability. Overall, the CCXs fall into 16 clusters, reflecting different patterns and drivers. Triple CCX are largely confined to the tropics and the North Pacific, and tend to be associated with the El Niño-Southern Oscillation.

Plain Language Summary

The global ocean is getting warmer, more acidic, and losing oxygen due to climate change. On top of this trend, sudden increases in temperature, or drops in pH or oxygen adversely affect marine organisms when they cannot quickly adapt to these extreme conditions. These conditions are worse for marine organisms when such extremes occur together in the vertical water column leading to a column-compound extreme (CCX) event, severely reducing the available habitable space. To investigate such CCXs, we use a numerical model simulation of the global ocean during the historical period of 1961 to 2020. Singular extreme events are identified primarily with relative percentile thresholds, while CCXs require a 50 m minimum depth threshold in the water column. We find that CCXs have been increasing in volume, occupying up to 20 % of the global ocean volume towards 2020. We then remove the climate trend to better understand the drivers behind CCXs. Many CCXs occur in the tropics and high latitudes, lasting 10 to 30 days and reducing habitable space by up to 75 %. This study is the first to systematically detect compound extremes in the water column, and forms the basis to determine their detrimental effects on marine organisms and ecosystems.

1 Introduction

Climate change has measurably warmed the ocean, increased its acidity, and decreased its oxygen content (Masson-Delmotte et al., 2021). These trends are punctuated by extreme events whose intensities and rapid onsets possibly impact marine organisms and ecosystems more than the slowly evolving trends do (Collins et al., 2019; Gruber et al., 2021). The study of marine extremes emerged forcefully in the last decade, with the vast majority of studies having focused on marine heatwaves (Hobday et al., 2016; Holbrook, Sen Gupta, et al., 2020; Oliver et al., 2021), their drivers (Holbrook et al., 2019; Sen Gupta et al., 2020), and impacts (Smale et al., 2019; K. E. Smith et al., 2023). But also ocean acidity extremes (OAX) (Hauri et al., 2013; Kwiatkowski & Orr, 2018; Negrete-García et al., 2019; Burger et al., 2020; Desmet et al., 2022) and low oxygen extremes (LOX) (Chan et al., 2008; Hofmann et al., 2011; Leung, Mislan, et al., 2019; Köhn et al., 2022) are receiving increasing attention, with the study of compound marine extremes, that is, events when conditions are extreme in more than one stressor emerging as an

issue of special concern(Gruber et al., 2021; Le Grix et al., 2021; Burger et al., 2022; Le Grix et al., 2022).

Such compounded extreme events can have a disproportionately large impact on marine biota, especially when the different stressors act synergistically, that is, when they reinforce each other (Crain et al., 2008; Boyd & Brown, 2015; Pirotta et al., 2022). A well-known example is the decrease of aerobic metabolic rates with increasing temperature and decreasing oxygen (Pörtner & Knust, 2007; Deutsch et al., 2015), making ectotherms especially susceptible to compounded MHW and LOX. Bednaršek et al. (2018) also showed biological implications for pteropods during anomalously high temperature and acidity events (the latter corresponding to anomalously low pH events, with pH = - log[H+], and [H+] being the concentration of the hydrogen ion). Extremes can be compounded in different ways that lead to amplified impacts on organisms and ecosystems. Multiple extremes occurring at the same time and place has been explored with properties such as temperature and pH (Burger et al., 2022), temperature and chlorophyll (Le Grix et al., 2021), pH and oxygen (Nam et al., 2011; Köhn et al., 2022), and for triple extremes involving pH, oxygen, and temperature (Gruber et al., 2021).

Warming of the ocean over the past 150 years and the strong trend in ocean acidification have lead to a substantial increases in the MHW and OAX extremes associated with these stressors (Oliver et al., 2018; Gruber et al., 2021) and are bound to increase in the future as long these driving trends continue (Frölicher et al., 2018). For example, Oliver et al. (2018) showed that between 1925 to 2016, the frequency and duration of MHW increased by 34% and 17%, respectively, resulting globally in a more than 50% increase in the number of MHW days. For OAX, the trends are even stronger, going from a pre-industrial situation with about 4 days with extreme conditions to a nearly permanent state of extremes (Gruber et al., 2021; Burger et al., 2022). Corresponding trends are also expected for the LOX extremes driven by ocean deoxygenation (Gruber et al., 2021), but the global ocean deoxygenation trends tend to be smaller compared to the level of variability, leading to smaller, and not yet well established trends in LOX. As a consequence of these trends in the single stressor extremes, compound extremes must increase as well. Gruber et al. (2021) attributed, for example, the development of widespread double compound extremes in the Northeast Pacific over the past 40 years, and especially the triple-compound extreme at the height of the "Blob" event, in part, to the underlying trends ocean warming, acidification, and deoxygenation. They speculated, that part of the broad ecological impacts of the "Blob" might be caused by these compound extremes. However, in order to understand the mechanisms driving the extremes, it is better to remove the trend in the extremes, by using a so-called moving baseline (Oliver et al., 2021; Burger et al., 2020; Gruber et al., 2021; Burger et al., 2022). Analysis of extremes, and especially compound extremes on a moving baseline is also appropriate when considering the impact of these extremes on organisms that have the capacity to adapt to the more slowly evolving changes in temperature, ocean acidification, and oxygen (see also discussion by Sen Gupta (2023)).

So far, the vast majority of MHW studies have focused on the surface ocean only, disregarding the fact that many organisms might have the potential to migrate to colder temperatures at deeper depths when a surface heat wave affects them (Jorda et al., 2020). Furthermore, the habitat of vertically migrating organisms can be considered to include the water column down to about 400 m (Bianchi et al., 2013; Bianchi & Mislan, 2016). Detecting extremes across the vertical dimension is thus an important step towards understanding the compression of habitable space during such extremes. Some MHW studies have looked into the subsurface, (Schaeffer & Roughan, 2017; Elzahaby et al., 2021; Scannell et al., 2020; McAdam et al., 2022; Fragkopoulou et al., 2023), while the concept of habitat compression has been considered with respect to temperature and oxygen changes (Jorda et al., 2020; Köhn et al., 2022). However, a consistent definition of compound extremes in the column has yet to be defined. The well-studied surface MHW

may extend into subsurface, compounding vertically with OAX and LOX to deteriorate the habitable conditions of the water column.

Marine extremes can be driven by various mechanisms, and the study of compounded extremes in the vertical dimension increases the complexity of this task (Gruber et al., 2021). Surface MHWs are understood to be primarily driven either from the atmosphere through anomalous air-sea heat fluxes, or by lateral heat advection (Sen Gupta et al., 2020; Holbrook, Sen Gupta, et al., 2020; Marin et al., 2022). Such surface MHWs may cause higher stratification in the upper ocean, suppressing the upwelling of carbon-rich and low-oxygen waters and hence, decreasing the likelihood of surface OAX and LOX. However, temperature anomalies have been shown to influence OAX occurrence by shifting the carbonate chemistry equilibrium or modulating dissolved organic carbon (DIC) (Burger et al., 2022), thereby increasing or decreasing $[H^+]$ respectively. At depth, vertical or lateral displacement of waters across strong gradients in temperature, $[H^+]$, or oxygen tends to be an important driver of extremes there, with the orientation of the gradients being key for determining the nature of the compounded extreme. But there are many other mechanisms, involving also biological physical interactions, e.g., in mesoscale eddies (Gruber et al., 2021; Köhn et al., 2022; Desmet et al., 2022) that are key for generating and maintaining marine extremes at depth. Considering the various physical, chemical, and biogeochemical processes in the ocean, inferring the mechanisms behind compound extreme events can be a complex task. Extremes which are compounded may share a common driver, be driven by one another, or co-occur in the column with different drivers (Gruber et al., 2021). With percentile thresholds, some detected compound extremes may arise purely out of statistical chance (Burger et al., 2022). Extremes with affiliated drivers have a higher propensity of co-occurrence above such a random signal. Such compound extremes are significant and merit investigation.

Extreme events across the globe have been linked to large scale climate modes, the dominant one being the El Niño-Southern Oscillation (ENSO) (Santoso et al., 2017; Holbrook, Claar, et al., 2020). The prevalence of ENSO in the study of marine extremes is partly due to the large area it affects in the Pacific, but also due to its teleconnections with other ocean basins (Roy & Reason, 2001; Luo et al., 2010). ENSO events are triggered by changes in the winds in the eastern tropical Pacific, but they affect, through connected changes in large-scale ocean and atmospheric circulations, many remote regions (aka teleconnections). While ENSO might not directly cause the extreme, the ENSO-driven changes in the mean state can make the occurrence of extremes more likely or prolong and intensify existing extremes. A good example is the 2013-2015 "Blob" marine heatwave in the Northeast Pacific, which turned into one of the world's largest and longest lasting MHW owing to the coalescence of regional circulation changes and ENSO-driven warming (Di Lorenzo & Mantua, 2016; Holbrook et al., 2019; Gruber et al., 2021). ENSO has also been linked to MHWs in the Indian and Southern oceans (Holbrook et al., 2019; Sen Gupta et al., 2020; Oliver et al., 2021). In addition, ENSO has been shown to strongly affect also OAX and LOX in the Pacific ocean, especially at depth (Turi et al., 2018; Leung, Thompson, et al., 2019; Köhn et al., 2022; Desmet et al., 2023).

Here, we extend the existing work on marine extremes by expanding our analysis simultaneously in two directions. We expand in depth by analyzing extremes across the whole upper water column, and we expand in terms of stressors by focusing on compound events. Thus, we will define, study and characterize, for the first time, column-compound extreme events in the vertical water column at the global scale, and aim to understand their drivers. To this end, we will use results from a hindcast simulation undertaken with a global ocean coupled physical/biogeochemical model, sampled at high temporal frequency to permit us to identify extremes. We rely on model simulation results since there are no observational records available across all parameters and especially not at depth that would permit us to undertake this study based on observations.

We also develop a framework to analyze such events, which we call Column-Single eXtreme events (CSX) in the case of a single parameter being extreme across a good portion of the water column, and Column-Compound eXtreme events (CCX), which are those events when more than one CSX is detected in the same column at the same time. We will show that these events are prevalent in the ocean, although primarily occurring in the low latitudes, and that their frequency, duration, and intensity have increased in recent decades. While we cannot identify the potential impacts yet of these extremes on marine organisms and ecosystems, the multi-dimensional nature of the extreme conditions are bound to push marine organisms to their limits. We will show the places and times where these column extremes tend to occur, giving insights into where and when one should look for these ecological impacts.

2 Detecting Extreme Events in the Water Column

No consistent definition of single or compound marine extreme events exists so far, much less if they are co-occurring in the same vertical column. We thus first review the issues at hand, and then illustrate the framework we have used to identify the Column-Single eXtreme events (CSX) and the Column-Compound eXtreme events (CCX).

A common issue to be resolved in all studies is the choice of thresholds and baselines. Regarding the threshold, the MHW-related studies have relied on a relative percentile threshold approach with the majority of studies using a seasonally-varying (Oliver et al., 2018; Holbrook, Sen Gupta, et al., 2020), so that extreme conditions can be detected regardless of the season. In contrast, absolute thresholds remain pertinent to extremes such as LOX, where the metabolic requirement for organisms tends to be fixed (Hofmann et al., 2011), with some degree of variability with temperature (Seibel, 2011; Deutsch et al., 2015). Absolute thresholds have also been used to detect extremes in aragonite saturation state (Hauri et al., 2013; Negrete-García et al., 2019; Desmet et al., 2022), where a thermodynamic threshold determines the state of dissolution of the shells of calcifying organisms. Thus, there are clear grounds for using either relative or absolute thresholds, and we make use of both in this study.

The baseline, i.e., the time-period used to identify the thresholds, is also a critical choice in detecting extremes (Jacox, 2019; Oliver et al., 2021; Sen Gupta, 2023). In the case of a fixed baseline, the thresholds remain invariant such that the trends in temperature, pH, and oxygen imply an increase in the frequency and intensity of extremes events (Gruber et al., 2021). This could be problematic when cold spells in later years are potentially marked as heatwaves (Jacox, 2019), or when waters become classified as permanently extreme with regard to ocean acidification (Hauri et al., 2013; Burger et al., 2020, 2022; Gruber et al., 2021). An alternative is the use of a moving baseline, i.e., where the reference period used to identify the relative thresholds is shifting in time with the analysis, or alternatively, where the thresholds are computed based on detrended data. An analysis with such a moving baseline gives equal weight to extreme events across the entire time period (Burger et al., 2020; Rosselló et al., 2023), and is more suitable for the investigation of drivers (Chiswell, 2022). It is also more relevant to organisms that are able to adapt to the gradually changing conditions (Holbrook, Sen Gupta, et al., 2020; Oliver et al., 2021), but are still affected by the sudden change in conditions during an extreme event. In this study, we first present our results on a fixed baseline, illustrating the response of extreme events to the climate trend. Then, we primarily use the moving baseline to analyse extreme events and postulate drivers. A quadratic moving baseline is chosen to fit the long term trend in H+] (Hauri et al., 2021) (Supporting Information Text S1 and Figure S1-S2).

The next choices concerns the vertical structure and the compounding. For the vertical structure, we define columns to be Column-single eXtreme events (CSX) of a particular type (MHW, OAX, or LOX) when the grid cells that are considered to be extreme

with regard to this particular parameter occupy more than 50 m of the upper 300 m of the water column. For the compounding, we identify columns to be Column-Compound eXtreme events (CCX) when more than one CSX is detected in the same column at the same time. This leads to three types of double stressor CCX, i.e., MHW-OAX, MHW-LOX, and OAX-LOX, and one type of triple stressor CCX, i.e., MHW-OAX-LOX.

In Figure 1a, a conceptual sketch of the various types of defined extremes is shown for a single column over time. Grid-cell extreme events are coloured within the Hovmoller diagram where they occur. However, this does not mean that a column extreme is occurring. For example, a CSX-MHW starts at day 20 from the surface, while a CSX-OAX and CSX-LOX start from the bottom of the column at days 35 and 47 respectively. The duration of the CSXs and CCXs are labelled with arrow ranges below Figure 1b.

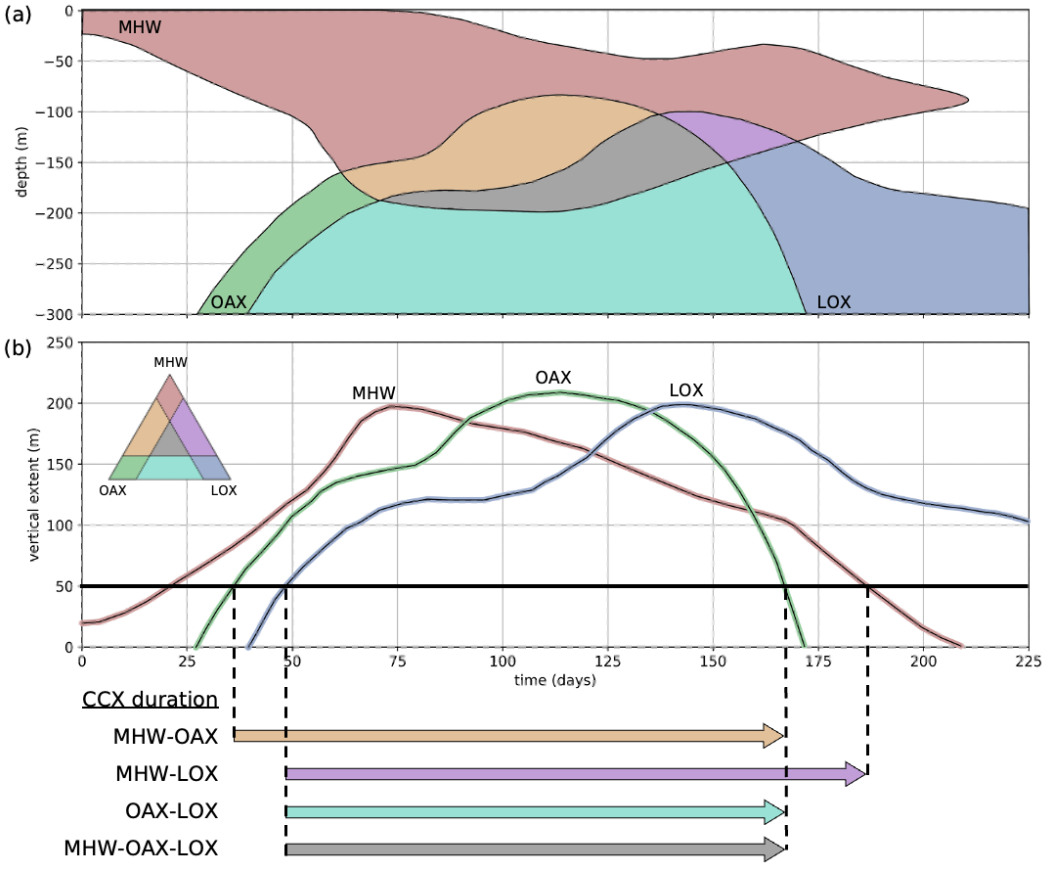

Figure 1. Illustration of the concepts used to detect and analyze column compound extremes. (a) Idealized Hovmoller diagram illustrating the time-depth evolution of extreme conditions in a hypothetical water column from the surface down to 300 m depth. The coloured regions within the plot are considered extreme, with the colors brown, green and blue representing pure MHW, OAX and LOX, respectively. The areas where the different extremes overlap are given colors according to the mixing diagram in panel (b). (b) Timeseries of the total vertical extent (within the top 300 m of the water column) for each extreme type. When the vertical extent for a particular type of extreme exceeds 50 m, then we call it a *Column-single eXtreme event* (CSX) of this parameter and when more than one of these occur at the same time a *Column-Compound eXtreme event* (CCX). The duration of the four different types of CCX is indicated by arrows.

3 Methods

3.1 Model Simulations

To identify the CSX and CCXs, we use results from a hindcast simulation performed with the ocean component of the global Community Earth System Model (CESM) Version 1.2 (Gent et al., 2011). The ocean component consists of the Parallel Ocean Program 2 (POP2) (R. Smith & Gent, 2010) simulating ocean circulation and mixing, of the Community Ice CodE 4 (CICE4) model, also known as the Los Alamos Sea Ice Model (Hunke & Lipscomb, 2008) simulating the presence and thickness of sea-ice, and of the Biological Elemental Cycling (BEC) model (Moore et al., 2004, 2013) representing ocean ecology and biogeochemistry. The model has a nominal meridional resolution of 0.5° near the poles, refining to 0.3° at the Equator, and a nominal zonal resolution of 1°. There are 60 depth levels in the vertical dimension, extending from the surface to 5375 m. BEC includes three phytoplankton functional types that are grazed by one zooplankton type. The temperature and dissolved oxygen fields are prognostic variables of the coupled model, while the hydrogen ion concentration (on the total scale) values were obtained from the model simulated inorganic carbon parameters by applying carbonate system calculations based on the OCMIP2 routines (Orr et al., 2005). Details of the model can be found in S. Yang and Gruber (2016).

The model simulations started from a spun-up preindustrial state (S. Yang & Gruber, 2016) and was brought forward from 1850 to 1957 with cyclically repeated monthly atmospheric forcing from the Japanese 55-year Re-analysis (JRA-55) product (Ebita et al., 2011) and atmospheric CO_2 prescribed according to observations provided by the Global Carbon Project (Friedlingstein et al., 2022). The hindcast simulation was then produced with daily output for the years 1958 to 2020 also using the monthly JRA-55 forcing. We discard the first three years, and thus limit our analysis to the 60-year period between 1961 and 2020. Results from this simulation were also used for the global Carbon Budgets 2020 and 2021 (Friedlingstein et al., 2022) and in the study by Hauck et al. (2020).

3.2 Extreme Events Detection

In the first step, single extreme events of MHW, OAX, and LOX are detected for each grid cell for each day. For MHW and OAX, a 95th percentile threshold is applied to the temperature and H^+ fields respectively, using seasonally varying thresholds. For LOX, we require the oxygen concentration to be below the 5th percentile value (again seasonally varying), and simultaneously to be less than 150 μM ($\sim$ 3.5 ml/L). The absolute threshold for LOX was added because LOX at high oxygen levels have very little biological impact. The value chosen is the hypoxic threshold of some larger fish species such as yellowfin and skipjack tuna, marlin, and sailfish (Braun et al., 2015; Leung, Mislan, et al., 2019; Rose et al., 2019). The detection thresholds for single events in the grid cell are summarised in Table 1. In this work, we do not impose any additional criteria such as minimum duration (Hobday et al., 2016), since the monthly forcing applied to the CESM hindcast prevents the formation of short duration events that may have to be filtered out. For the fixed baseline thresholds, the data are detrended with a quadratic trend to a reference year of 1958 prior to computing the percentile thresholds. For the moving baseline results, the thresholds change with time with respect to the fitted quadratic trend.

Table 1. Single extremes and the thresholds used for their detection

Single Extreme Type	Variable	Percentile Threshold	Additional Absolute Threshold
Marine Heatwave (MHW)	T	$> 95^{\text{th}}$	-
Ocean Acidification Extreme (OAX)	$[H^+]$	$> 95^{\text{th}}$	-
Low Oxygen Extreme (LOX)	$[O_2]$	$< 5^{\text{th}}$	$< 150\,\mu$M

To define extreme events in the vertical column, we require at least 50 m out of the top 300 m to be extreme with respect to each stressor. The analysis range of 300 m reflects the vertical habitat range of epipelagic and other vertically migrating organisms (Bertrand et al., 2010; Bianchi et al., 2013; Bianchi & Mislan, 2016). The value of the minimum extension of 50 m is somewhat subjective, but aims to capture the occasion when a substantial fraction of the water column is extreme, affecting the organisms living within this water column in a major way. Adjusting this minimum extension modulates the number of column extremes detected, but does not significantly change their spatial or temporal distribution (Supporting Information Test S2 and Figures S3-S6). When the 50 m vertical threshold is met for a single stressor, it is denoted as a column-single extreme event (CSX), illustrated in Figure 2a. The criteria for a CCX is met when two or more CSXs occur in the same vertical column, at the same time. Various configurations of CCXs are illustrated in Figure 2b. CSXs can be separately located in the column (c), or have some overlap (e). The single extreme grid cells do not need to be connected vertically to meet the 50 m threshold, as seen in (b) and (d). Under our definition of CCXs, triple compound events of MHW-OAX-LOX are also always double CCXs, and are included in their metrics.

3.3 Extreme Event Metrics

The metrics used to characterise extreme events can be broadly grouped into frequency, intensity, and temporal categories. With regard to extremes in the vertical column, we also quantify their size, location, and remaining continuous habitable space (see Table 2). While many of these metrics are commonly used in extreme studies, some had to be redefined in the context of our work on column extremes. We do not include severity in our analyses, i.e., the cumulative sum of the intensity value over the duration of the event (Hobday et al., 2016; Hauri et al., 2013; Samuels et al., 2021) since it strongly correlates with the event duration.

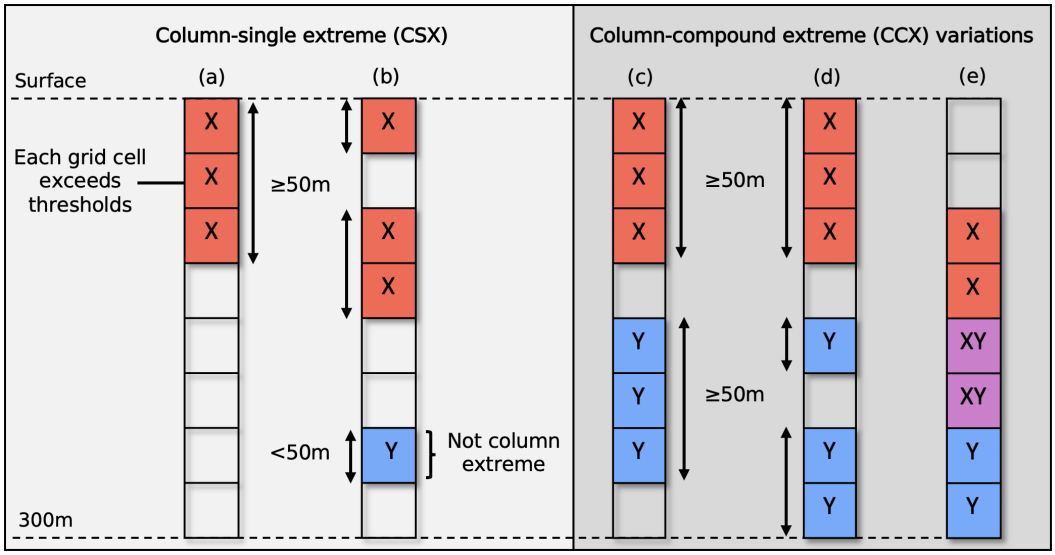

Figure 2. Illustration of different types of column-extreme events within the water column. (a) Column-single extreme (CSX), (b) CSX with discontiguous grid cells of extreme type 'X', (c) Column-compound extreme (CCX), (d) CCX with discontiguous grid cells of extreme type 'Y', (e) CCX with overlapping 'X' and 'Y' type extremes.

Table 2. Metrics used in the analysis of extreme events

Name	Symbol	Definition
Frequency metrics		
Days per year	N	Mean number of extreme days per year
Co-occurrence propensity	CP	Likelihood of two or more CSXs occurring within the same vertical water column at the same time
Enhancement (Suppression) of CCX during ENSO	ΔN	Mean increase (decrease) in number of extreme days per year during ENSO events, compared to that in the neutral phase
Intensity metrics		
Intensity index	ψ_i	Ratio of an event variable's i difference from its climatological value to the difference between the threshold and climatological value
Compound intensity index	Ψ	Square-root of the sum of squares of the intensity index of individual events, that make up a compound event
Maximum intensity index	$\psi^{\max}$	Maximum value of the intensity index over time and the vertical column
Temporal metrics		
Duration	D	Lifetime of an event for which the thresholds are met continuously
Size and location metrics		
Volume fraction	f_V	Fraction of total volume of a defined region that is affected by the specified extreme type
Vertical fraction	f_z	Fraction of top 300 m occupied by extremes
Contiguous habitable space fraction	f_h	Fraction of the top 300 m contiguously unaffected by extremes

The duration of an event refers to the total length of time for which the specified extreme type exists in the water column. For example, a MHW-OAX event starts from the time CSX-MHW and CSX-OAX both exist in the water column, even if the CSX-MHW started earlier (see Figure 1). The same applies to the end of a CCX.

The intensity index expresses the strength of a extreme event in a unitless fashion. It is inspired by the MHW categories of Hobday et al. (2018), and defined as the continuous severity index by Sen Gupta et al. (2020). Using the intensity index as a measure of event intensity permits us to compare the intensities of multiple extreme and even to combine them. For a single grid cell it is expressed as:

$$\psi_X = \frac{X - X_c}{X_t - X_c}, \tag{1}$$

where X is the parameter of interest, X_c is its climatological value for that day of the year, and X_t is the threshold value. For the climatology, we use the median value in order to prevent it from being skewed by exceptionally intense extreme events. Th median value is obtained from a seasonally-varying 11-day rolling window. To express the intensity index of a multiple extremes occurring in the same grid cell, we take the Euclidean norm of ψ of the single extremes:

$$\Psi = \sqrt{\psi_X^2 + \psi_Y^2 + \psi_Z^2}, \tag{2}$$

where ψ_X, ψ_Y, and ψ_Z are the intensity index values of single extremes.

The co-occurrence propensity (CP) is a central metric for the study of compound extremes as it permits us to assess whether two extremes co-occur by chance, or whether they co-occur as a result of a common process forcing them. Likewise the propensity can be used to assess whether two extremes co-occur much less frequently than expected by chance, since the common process actually leads to conditions that suppress the co-occurrence. The CP metric is defined as the likelihood of two (or three) different CSXs occurring in the vertical column at the same time. It is scaled to the range of [-1,1]. A value of 1 indicates the CSXs always occur together whenever they occur, while a value of -1 indicates that they never occur together. A value of 0 suggests that their occurrences are independent, as if randomly distributed in time. A high value suggests that the CSXs in consideration have similar or related drivers, while a low value suggest that they have opposing drivers. The CP metric is similar in concept to the likelihood multiplication factor (Zscheischler & Seneviratne, 2017).

First, the independent (random) value of CCX days per year is computed using the mean number of CSX days per year:

$$N_r = \begin{cases} \frac{N_1}{D_Y}\frac{N_2}{D_Y} \times D_Y, & \text{for double extremes,} \\ \frac{N_1}{D_Y}\frac{N_2}{D_Y}\frac{N_3}{D_Y} \times D_Y, & \text{for triple extremes,} \end{cases} \tag{3}$$

where N_1, N_2, N_3 are the mean number of days per year of different CSXs, and $D_Y = 365$ is the number of days in a year. The CP metric is then defined as:

$$\mathrm{CP} = \begin{cases} \frac{N - N_r}{N_{\max} - N_r}, & N > N_r \\ \frac{N - N_r}{N_r}, & N < N_r \\ 0, & N_r = 0 \end{cases} \tag{4}$$

where N is the mean number of days per year of the CCX, and $N_{\max}$ is the global maximum value of N. Since CP is proportional to the mean number of days of extremes, it is also representative of the annual number of days.

3.4 Clustering of Extremes

In order to find commonalities of the detected CCXs with regard to their vertical structure and to assist us in identifying the underlying drivers, we cluster the detected CCXs with a k-means clustering approach (MacQueen, 1967). The clustering algorithm is performed on the vertical locations of single extreme events in the column, exclusively during CCXs and for grid cells with a positive co-occurrence propensity. In detail, the water column is first divided into 6 bins of 50 m each, and then, over the 60 year analysis period the number of occurrences of single extremes in each bin during CCXs is counted and weighted with their intensity index. These bins of vertical locations are then used as the dimensions of the clustering, with 12 dimensions for the double CCXs, and 18 dimensions for the triple CCX. These dimensions are chosen as the vertical locations of single extremes reflect the conditions under which they occur, and allude to their drivers. Further information about the clustering approach and choice of number of clusters is provided in the Supporting Information Text S3 and Figure S10.

3.5 Model Evaluation

Given our relying on model simulation results for detecting single and compound extremes across the upper water column, it behooves us to evaluate the model with regard to its ability to represent extremes. But our evaluations are largely limited to the surface. For MHW, we use the observations of sea-surface temperature from the Operational Sea Surface Temperature and Sea Ice Analysis (OSTIA) product (Good et al., 2019, 2020). covering the period 1982 to 2020. For OAX, we rely on the OceanSODA-ETHZ dataset (Gregor & Gruber, 2021) that covers the period 1982 to 2020. Surface MHW and OAX are detected in the monthly means of the observational products with a seasonally-varying 95th percentile threshold on a quadratic moving baseline, analogous to how this was done for the model output (see section 3.2). As ENSO turns out to be a major driver for the variability in extremes, we evaluate the model also with regard to ENSO, using the Oceanic Niño Index (ONI) and the depth of the $20°C$ isotherm across the equatorial Pacific.

The model captures the observed variations and global coverage of surface MHWs with high fidelity (Figure 3(a)). In particular, the model captures well the strong year-to-year fluctuations, which tend to be closely coupled to ENSO. The model also correctly simulates the distribution of the mean duration of these surface MHWs, especially the long MHW durations found in the eastern tropical Pacific. However, there is a slight tendency for the model to overestimate the duration, particularly in the extratropics (Figure 3(b)). This is common shortcoming of models (Frölicher et al., 2018; Gruber et al., 2021; Köhn et al., 2023) and while there are clearly issues with the models, it is also feasible that the observations tend to underestimate the duration owing to observational gaps. Finally, the model also represents the intensities of the surface MHW with great fidelity, both with regard to the absolute values and distribution (Figure 3(b)). We thus concluded that the model is performing very well with regard to the representation of the large and long-duration MHW at the surface.

The evaluation of surface OAXs with the observation-based product OceanSODA-ETHZ (Gregor & Gruber, 2021) produces somewhat more mixed results. However, one needs to note that the uncertainties associated with this product are much larger than those associated with SST. This is a consequence of the several orders of fewer observations that are available to construct a space-time distribution of pH or $[H^+]$. Still, the model-based timeseries of the global area coverage of surface OAX (based on $[H^+]$) agrees

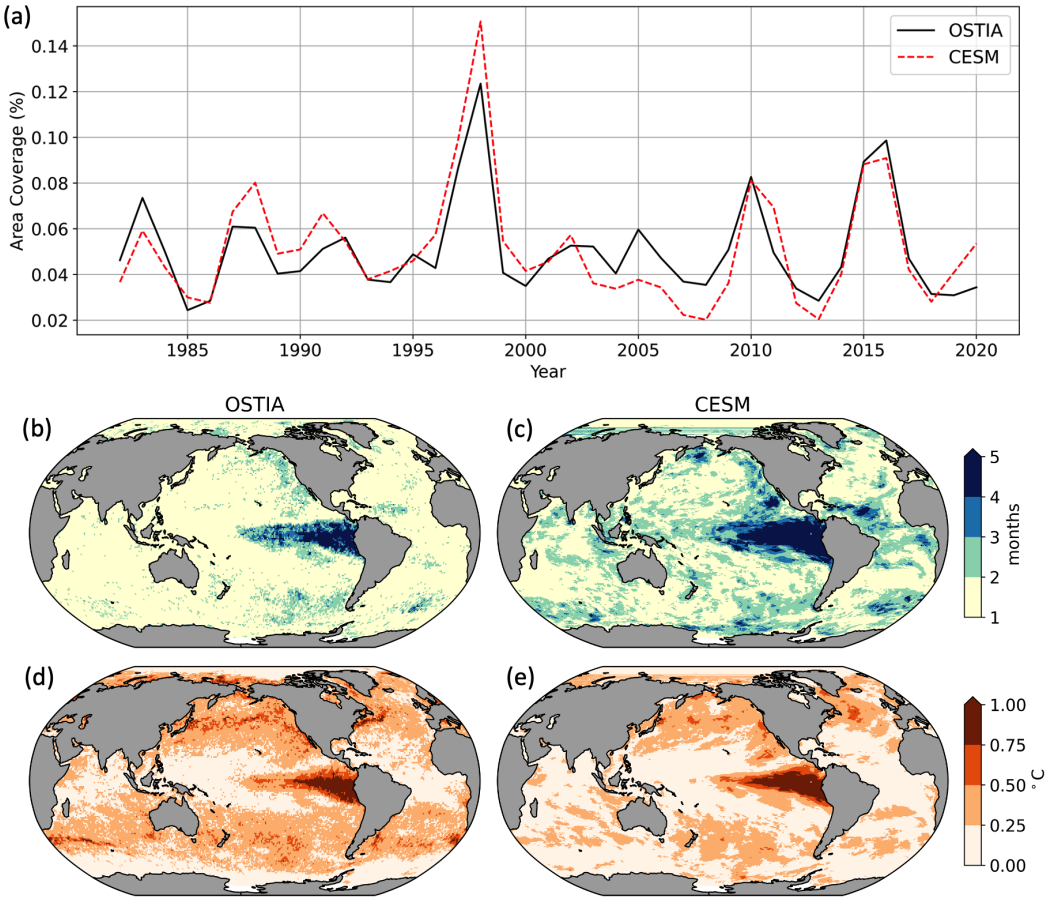

Figure 3. Evaluation of the hindcast model CESM with regard to its representation of surface marine heatwaves (MHW).(a) Timeseries of annual global area coverage of surface MHW identified by the OSTIA observational product compared to those diagnosed in the CESM hindcast. (b) OSTIA and (c) CESM mean duration of surface MHW. (d) OSTIA and (e) CESM mean annual maximum MHW intensity. The MHW were diagnosed in the observations in the same manner as done for the model.

remarkably well with that inferred from the observation-based product, both in terms of mean and year-to-year variations (Figure 4(a)). However, the peak values differ by up to about 50%, with this difference being especially apparent in the years 1988-1989 and 1997. The surface OAXs detected with CESM have a similar pattern as that inferred from the observation-based product, especially with regard to the locations of the longest and most intense OAXs that are found in the tropical Pacific (Figure 4(b) and (c)). However, there is a mismatch in the high latitudes, especially in the North Pacific and Southern Ocean, where the model identifies long-lasting and intense surface OAX events, while they are not detected in the observation-based product. We suspect that this difference is most likely a consequence of the observation-based product underestimating the variability of $[H^+]$, thus detecting fewer and less intense OAXs. It also might be a consequence of biases in the model. Regardless, biases in the intensity tend to have only a minor effect on most conclusions drawn in this study, especially not with regard to the propensity or the mechanisms. Biases in intensity will impact, though, any derived metric, such as the compound intensity index of compound-OAX events.

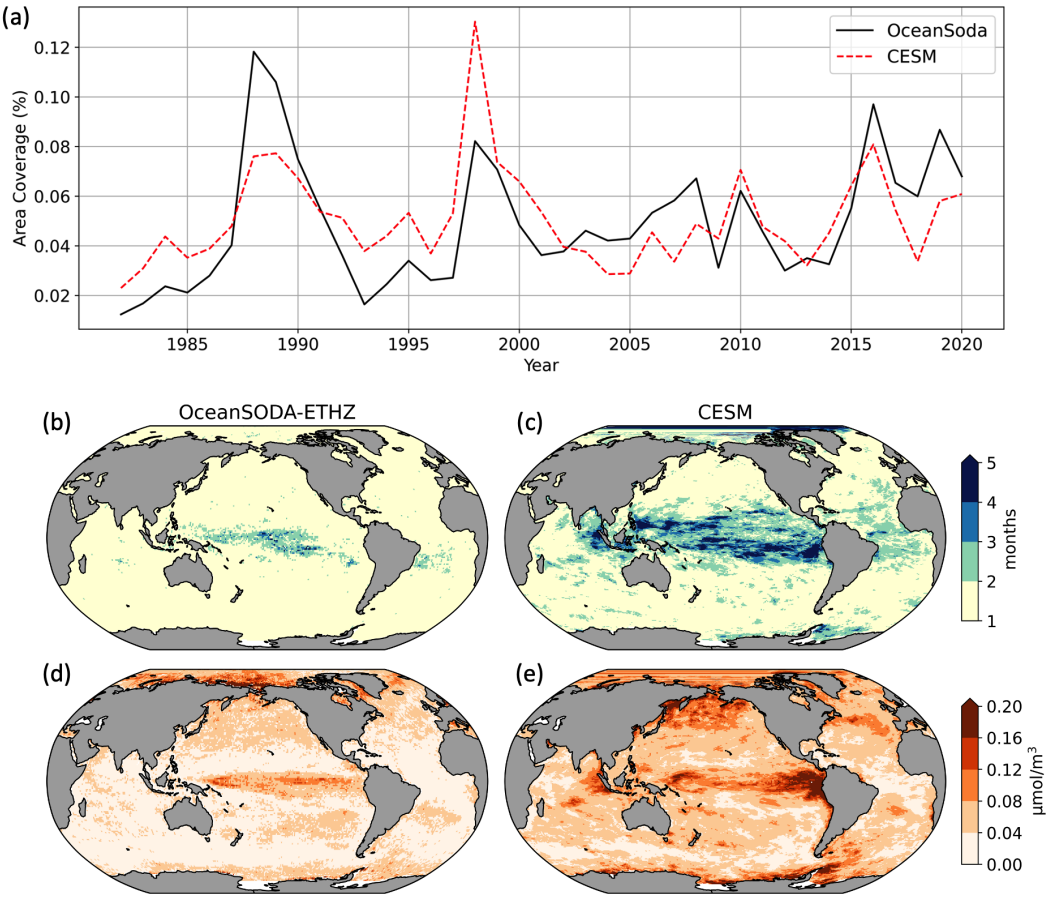

Figure 4. Evaluation of the hindcast model CESM with regard to its representation of surface ocean acidification extreme events (OAX) (a) Time-series of annual global area coverage of surface OAX identified on the basis of the OceanSODA-ETHZ observational product (Gregor & Gruber, 2021) compared to those diagnosed in the CESM hindcast. (b) OceanSODA-ETHZ and (c) CESM mean duration of surface OAX. (d) OceanSODA-ETHZ and (e) CESM mean annual maximum OAX intensity.

The hindcast model is doing an excellent job in simulating not only the time-series of the Oceanic Niño index ONI (bias of 0.11 °C, and correlation coefficient of $R^2 = 0.91$, based on ORAS5 (Zuo et al., 2019)), but also the variation of the thermocline structure in the eastern Pacific. Concretely, we assess the ability of the model to reproduce the depth of the 20 °C isotherm at monthly resolution (Supporting Information Figure S7). The interannual variability of the isotherm depth is comparable between the two, and the time scales of ENSO events are similar. We find a weaker zonal gradient in the CESM hindcast during ENSO events. This is likely due to a dampening of its SST variability due to a lower spatial resolution and monthly atmospheric forcing. But we overall conclude that the hindcast model is able to capture not only the mean state of the ocean's physical and biogeochemical state, but also its variability, which is a critical requirement to investigate extremes.

4 Results and Analysis

4.1 Trends of Column Extremes

Our model simulations reveal that the volumes occupied by column extremes for single parameters, i.e., CSXs and particularly those for OAX and MHW, have increased substantially over the 60 years of our analysis (Figure 5a). Their volume fractions started from values of a few percent in the 1960s and doubled for LOX, more than quadrupled for MHW to more than 20%, and reached nearly 100% for OAX by the end of the simulation in 2020. As these metrics were computed with a fixed baseline reflecting the conditions of the 1950s, these increases are a direct consequence of the underlying changes in temperature, oxygen, and acidity. The rapid changes in OAX and the more moderate increases in MHW diagnosed for the column extremes mimic the results obtained for the surface (Oliver et al., 2018; Burger et al., 2020; Gruber et al., 2021). This reflects the fact that ocean warming and ocean acidification are not limited to the surface, but are extending over much of the upper ocean (Gleckler et al., 2016; Kwiatkowski et al., 2020), causing strong trends also in column extremes. The trend in LOX events are comparatively muted because of smaller trends in oxygen and because of the additional absolute threshold of 150 μM used in this study.

The increasing volume fraction of single parameter CSXs causes also the volume fraction of column compound extremes (CCX) to increase, but the increases are less steep and also not as monotonic (Figure 5b). In the 1960s and 1970s, the volume fractions of the different combination hover around 0.1-1%, with the OAX-LOX events being the most prevalent at around 1%, and the triple compound extreme occupying less than 0.1% of the water column, on average. But then at various points in time, the prevalence of these CCX suddenly increased, such as is the case for the MHW-OAX extremes around 1980, from where the volume fraction increased to almost 25 % in 2020. The volume fraction of OAX-LOX jumped up around 1995, and then remained fairly constant near 5 %. The smallest increases are seen for the volume fraction of MHW-LOX and MHW-OAX-LOX, but they still increased by 2 and 24 times when comparing the first and last 20 years.

As the volume of CCXs has increased over the last 60 years, their duration has increased as well (Figure 5c). MHW-OAX and OAX-LOX events lasted on average less than 50 days before $\sim$1995, but jumped up in 1997. Thereafter, the mean duration of these CCXs rarely fell below 50 days and instead, achieved new records with durations of close to 200 days. MHW-LOX and the triple compound events have also increased in duration over the hindcast period, averaging close to 50 days per event towards 2020.

The starkest changes in the CCX properties occurred with the maximum intensity index (Figure 5d). In the 1960s and 1970s, it hovered around 2 for all compound extremes, except for OAX-LOX. But then, as the intensity of the OAX began to increase rapidly owing to the strong trends in ocean acidification (Ma et al., 2023), the maximum intensities of all CCX began to increase rapidly as well, reaching a nearly 10 fold increase by 2020. The exception are the MHW-LOX, which experienced "only" a doubling in their maximum intensity.

In summary, column compound extremes used to be relatively rare, but have become much more prevalent and frequent over the last few decades, and, in particular, have become much more intense. This is best illustrated for the triple column compound extremes that have expanded 24-fold, now last 3-times longer, and have become 6-times more intense since the early 1960s. The 0.45% of the volume of the global upper ocean being under conditions of triple compound extremes in recent years corresponds to 450 km^3 of the ocean. This is much larger than e.g., the volume of the ocean that is considered "dead" as a consequence of coastal eutrophication (Diaz & Rosenberg, 2008). Thus, while many studies have already shown the increasing frequency, duration, and intensities of surface extremes, especially those of MHW, our work now shows that this leads to se-

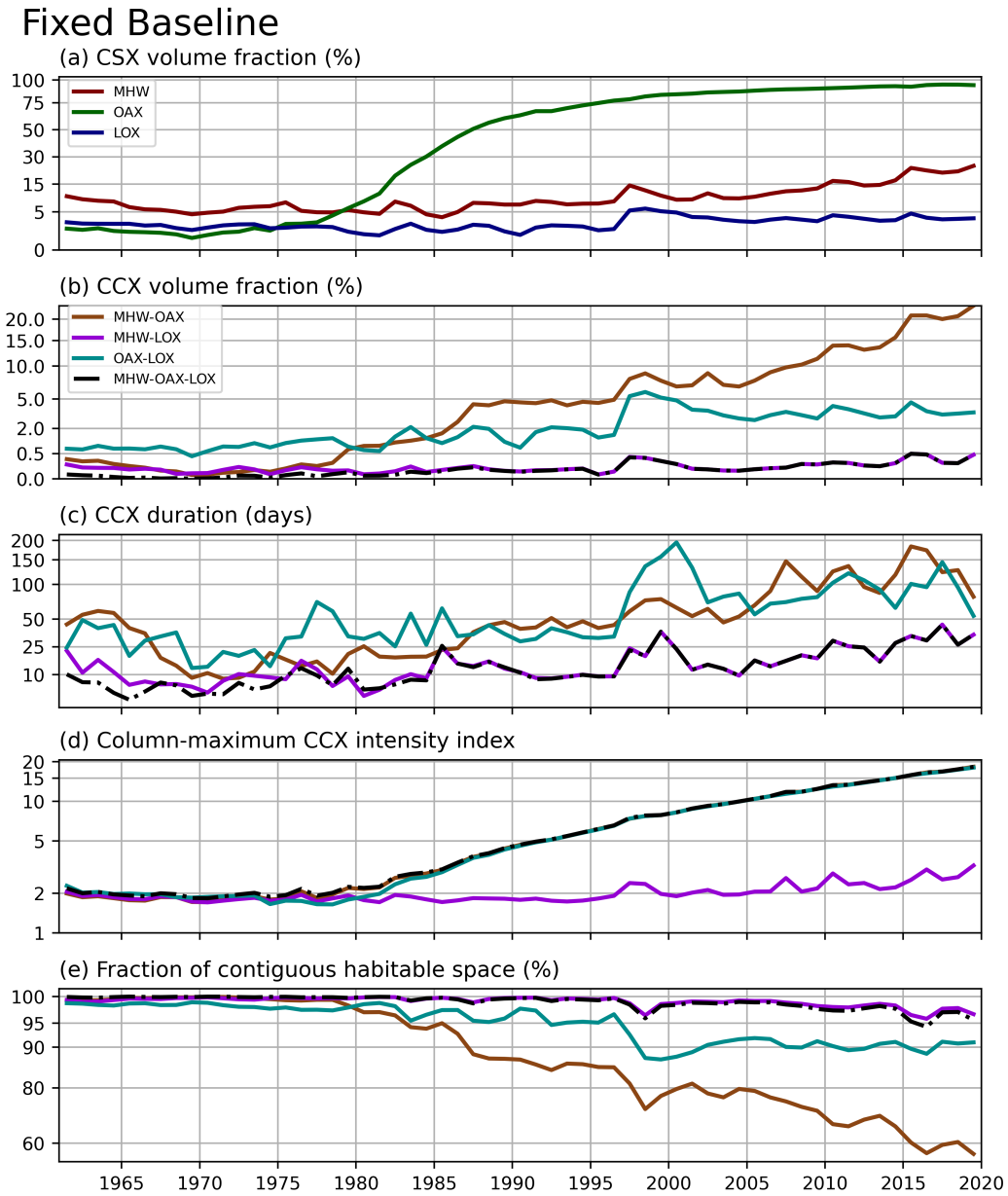

Figure 5. Temporal evolution of model simulated column extremes over the past 60 years on a fixed baseline. Shown are the timeseries of (a) annual mean global volume fraction of the three single column extremes (CSX), (b) annual mean global volume fraction of column compound extremes (CCX) of the four different types, (c) mean CCX duration, and (d) annual column-maximum CCX intensity index.

vere reductions in habitable space below the surface, restricting the capability of organisms to cope with e.g., surface MHW by by migrating to deeper depths. These analyses also show how important it is to better understand the impact of compound extremes on marine organisms, as these compound extremes are getting common.

Next, we would like to investigate the processes behind these events, and also understand what causes, e.g., also the strong year-to-year variations in the trends. We also

would like to characterize the events more specifically with regard to where they occur and what properties they have. To this effect, we change our perspective to a moving baseline which removes the long-term trend. We do this without the intention of understating the increasing severity of marine extremes under climate change.

4.2 Temporal Variability of Column-Compound Extremes

By removing the underlying climate trend through the use of a moving baseline, the strong year-to-year variability of the column-compound extremes become clearer (Figure 6). In particular, local peaks in global volume fraction, duration, and intensities of CCX coincide with ENSO events of high Oceanic Niño index (ONI). Most visible are the alignments of the peaks during moderate and strong ENSO events in 1972-1973, 1982-1985, 1997-1998, 2009-2011, and 2015-2016. In the tropical Pacific, we find that the volume fraction of double CCXs has a high Spearman correlation coefficient of >0.72 with El Niño events ($|\text{ONI}| > 0.5\,°\text{C}$, indicating that these events are likely to be driven by El Niño. The triple compound extremes have a lower correlation of 0.33 with El Niño. With La Niña, we find an asymmetric relationship with CCX volume fraction as compared with El Niño, with relatively weaker correlations. The highest coefficients of 0.37 and 0.35 are found for the triple CCX and for MHW-LOX, respectively, reflecting also the high interannual correlation of the triple CCX with MHW-LOX. OAX-LOX is correlated with La Niña with a coefficient of 0.26 , while MHW-OAX does not demonstrate any significant correlation. While ENSO can be identified as a major driver for many CCXs, especially in the tropical Pacific, it is also correlated with CCXs in other parts of the globe. We look into the correlation on a regional scale in Section 4.5.

OAX-LOX events affect the water column more than any other type of CCX. On average, they have the highest volume fraction of 0.73% ($735\,\text{km}^3$), reaching up to 3% ($3000\,\text{km}^3$) during the strong consecutive El Niño/La Niña events of 1997-1998. They also have the longest duration, lasting about 18 days on average, but exceeding 40 days during some periods. Due to their large volume, they also contract the habitable space the most out of all the CCX types.

The second most extensive type of CCX is MHW-OAX occupying typically about 0.3% of global volume ($280\,\text{km}^3$), and lasting 11 days on average. Together with the triple CCX, they are also one of the most intense CCX types, with an intensity index typically close to 2. While some peaks may be seen coinciding with major ENSO events, their association with ENSO is weaker than that of OAX-LOX. Finally, there is a relatively smaller volume of MHW-LOX and the triple CCX (MHW-OAX-LOX) during most years, of 0.038 % and 0.012 % respectively, corresponding to $38\,\text{km}^3$ and $12\,\text{km}^3$. These two CCX types have the same interannual variability, suggesting that many MHW-LOX events are also triple compound events.

4.3 Spatiotemporal Distribution of Column-Compound Extremes

The four different types of CCXs have a rather different global distributions in terms of the annual CCX days, i.e., the average number of days per year a particular location is characterized as a CCX (Figure 7a,c,e,g), and in terms of the co-occurrence propensity (Figure 7b,d,f,h). MHW-OAX occur globally, but most frequently in the subtropics and the high latitude Southern Ocean where typically about one week per year is characterized by a MHW-OAX event. In contrast, the number of MHW-OAX extreme days in the equatorial regions is low, and typically less than a week. The OAX-LOX events have nearly the opposite pattern. They occur primarily in the tropics, in the EBUS, and the north sub-polar Pacific with typically more than two weeks per year being under CCX conditions. No OAX-LOX CCX are detected in the North Atlantic and the ocean south of about 30°S. Compared to these first two CCX types, the MHW-LOX and the triple compound occur substantially less often, and last typically less than 7 days. The spa-

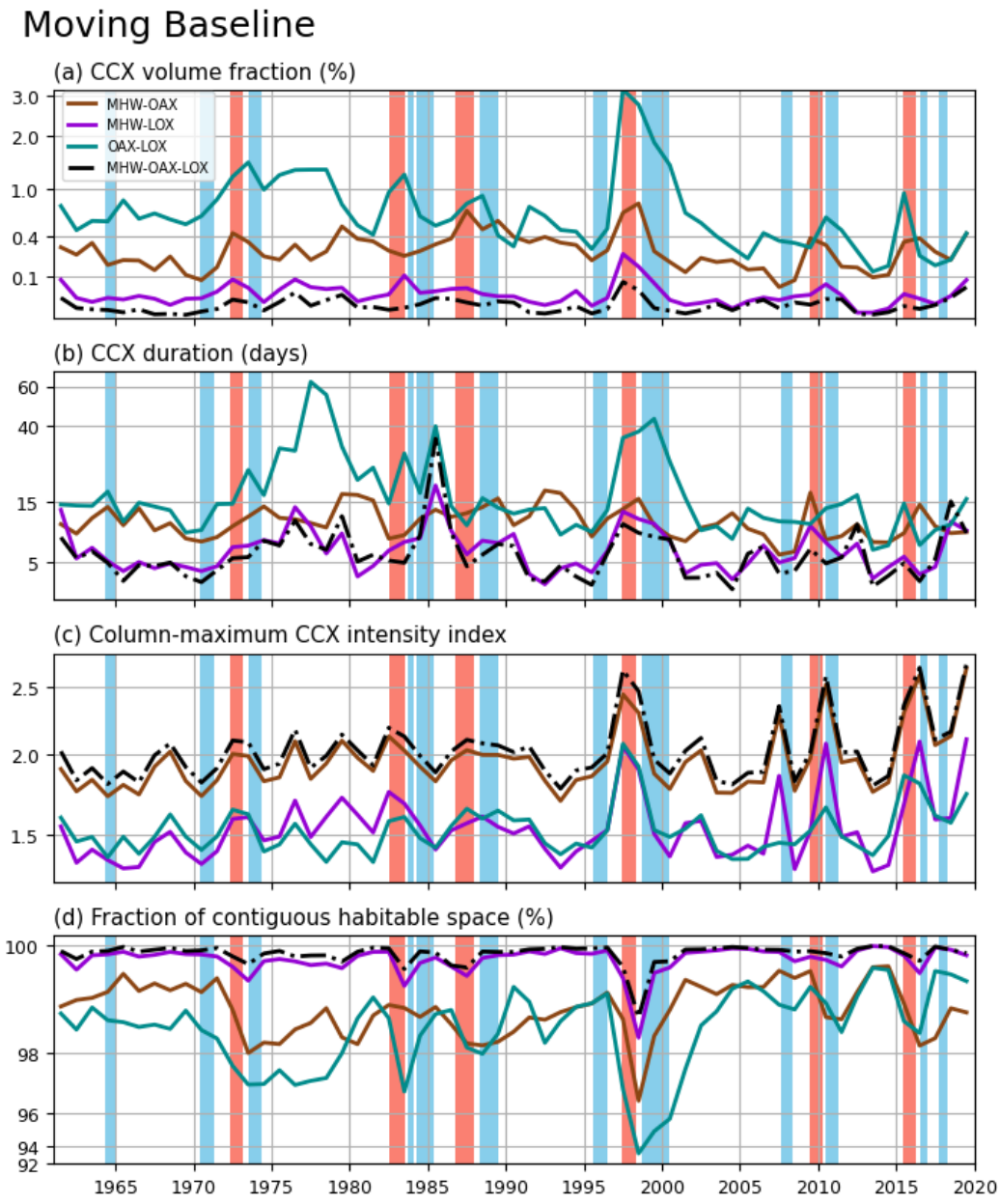

Figure 6. As Figure 5, but for a moving baseline, i.e., when the trends are removed using a quadratic fit. Strong El Niño events (ONI $\geq 1.5\,^{\circ}$C) are shaded in red, and strong La Niña events (ONI ≤ -1.0 are shaded in blue.

tial pattern is similar to that of the OAX-LOX extremes with a low-latitude focus. Their similar distributions are due to the close association of OAX with LOX, such that a majority of MHW-LOX are also MHW-OAX-LOX.

The co-occurrence propensity (later referred to as just propensity) helps to explain elements of these distributions. For example, the strongly negative propensity of the MHW-OAX events in the eastern tropical Pacific explains well why the number of CCX days in this region is so low (Figure 7a,b). This negative propensity means that whenever there is e.g., a heatwave in this region, the likelihood that this region has also an OAX is sub-

stantially lower than by chance. This can occur, for example, when heatwaves suppress the formation of OAX events. The very positive propensity for the OAX-LOX extremes in the tropics helps also to understood the high number of extreme days there. This means that when the region is characterized by either one of the two extremes, the likelihood of the other occurring is much higher than by chance. This can occur when the processes governing the development of these extremes are closely coupled. The much lower number of extreme days for the MHW-LOX and the triple compound extremes is also a consequence of the many regions with very negative propensity.

Thus, we can identify two overall patterns of CCX occurrence and propensity. A more global and high latitude pattern for MHW-OAX extremes, and a more low latitude/tropical pattern for the other three CCX types. This permits us in the following discussion of the full sets of metrics of the CCX to focus on just two of the four types, i.e., the MHW-OAX events (Figure 8) and the MHW-OAX-LOX triple compounds (Figure 9). The figures for the other two CCX types, i.e., OAX-LOX and and MHW-LOX may be found in the Supporting Information Figures S8-S9.

MHW-OAX events in the subtropics and Antarctic zone last the longest (more than 21 days) (Figure 8a). In these regions we also see the highest intensity index of 2 to 4 (Figure 8b), which means that the intensity of combined events are roughly 2 to 4 times the intensity of the threshold. This shows that where MHW-OAX occurs most frequently, they are also long and intense. Likewise, in the tropical regions where the number of CCX days is small and where the CCX events are short (Figure 8a, c) they are also relatively weak. This is also the region of very low propensity (Figure 8d). But when the CCX events are frequent, long and intense, they contract the habitable space moderately, between 25 % to 75 % of the column (Figure 8e). Meanwhile we see the highest contraction in the tropics between 50 % and 100 % of the column.

The spatial distribution of the triple compound event (MHW-OAX-LOX) can be understood in conjunction with that of OAX-LOX. OAX-LOX is unique from the other CCX types due to its high number of days per year (Figure 7c), and positive propensity everywhere it occurs (Figure 7d). This means that when either OAX or LOX occurs, the other almost always occurs together with it. The triple compound thus occurs when a MHW in induced in the same column. We see this most frequently in the tropics and the Bering sea, up to 21 days per year in some areas (Figure 9c). When they occur, they typically have moderate intensity index of 2 to 3, but exceeds 4 in the central tropical Pacific (Figure 9b). In the equatorial regions, they typically last up to 10 days (Figure 9c). However, their durations are more than double in the Bering sea and on the boundaries of the subtropical gyres. By far the triple compound event contracts habitable space the most (Figure 9f), by at least 50 % everywhere, and close to 100 % in some areas.

The key metrics for all the other events may be found in the Supporting Information (Figure S8-S9).

4.4 Vertical Structure and Clustering of CCXs

Next, we use the results of the k-means clustering of the CCXs in order to identify commonalities across the global ocean, helping us also to link the occurrence with potentially underlying processes. In the clustering, only those regions with a positive co-occurrence propensity were considered, i.e., where the likelihood of occurrence was larger than by chance (Figure 7). Even though the only information used for the clustering was the vertical distribution of the extremes, the resulting clusters (see Figure 10) also share similarities with regard to the intensity, duration, or frequency of the CCX, supporting our choice of the primary clustering variable.

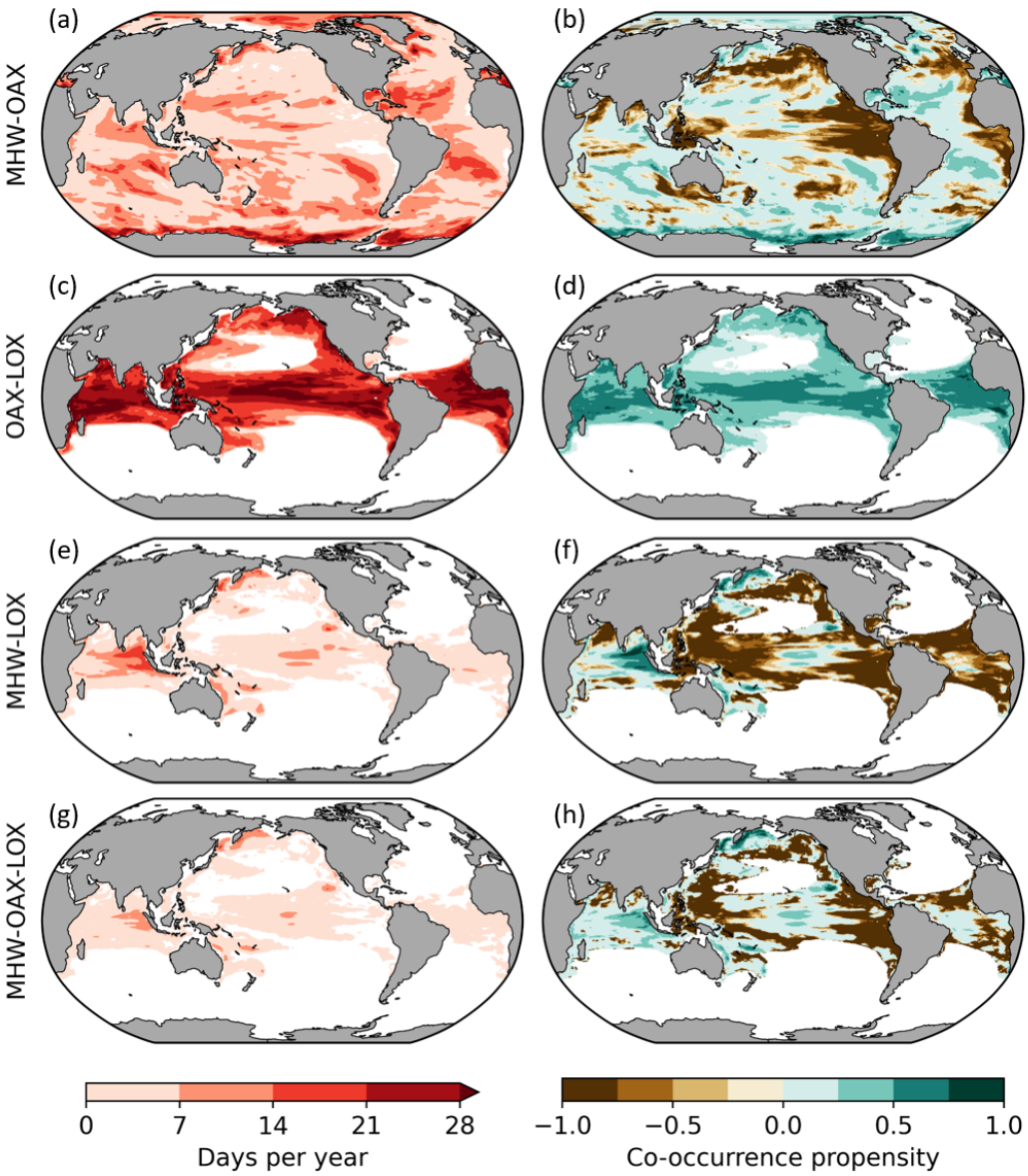

Figure 7. Spatial distribution of CCX illustrated by: CCX days per year (left column) and mean co-occurrence propensity of CCX (right column). The co-occurrence propensity represents the propensity of two column-single extremes occurring in the same column (Section 3.3). Each row corresponds to one CCX type, i.e. (a,b): MHW-OAX, (c,d): OAX-LOX, (e,f): MHW-LOX, (g,h): MHW-OAX-LOX.

The clustering for the MHW-OAX events results in four clusters (see Figure 10 left column). Clusters 2, 3, and 4 roughly correspond to the Subtropics, Subantarctic zone, and Antarctic zone. Cluster 1 covers the largest area by fraction (57.5 %). However, it also has the shortest duration, lowest days per year, and lowest intensity index. On the contrary, cluster 4 is the highest in these metrics.

Across all clusters (even that of other CCX types), MHW-OAX clusters 1 and 2 stand out as the only CCXs whose component extremes (MHW and OAX) are intensified simultaneously at the surface, occupying about 40 % of the water column on av-

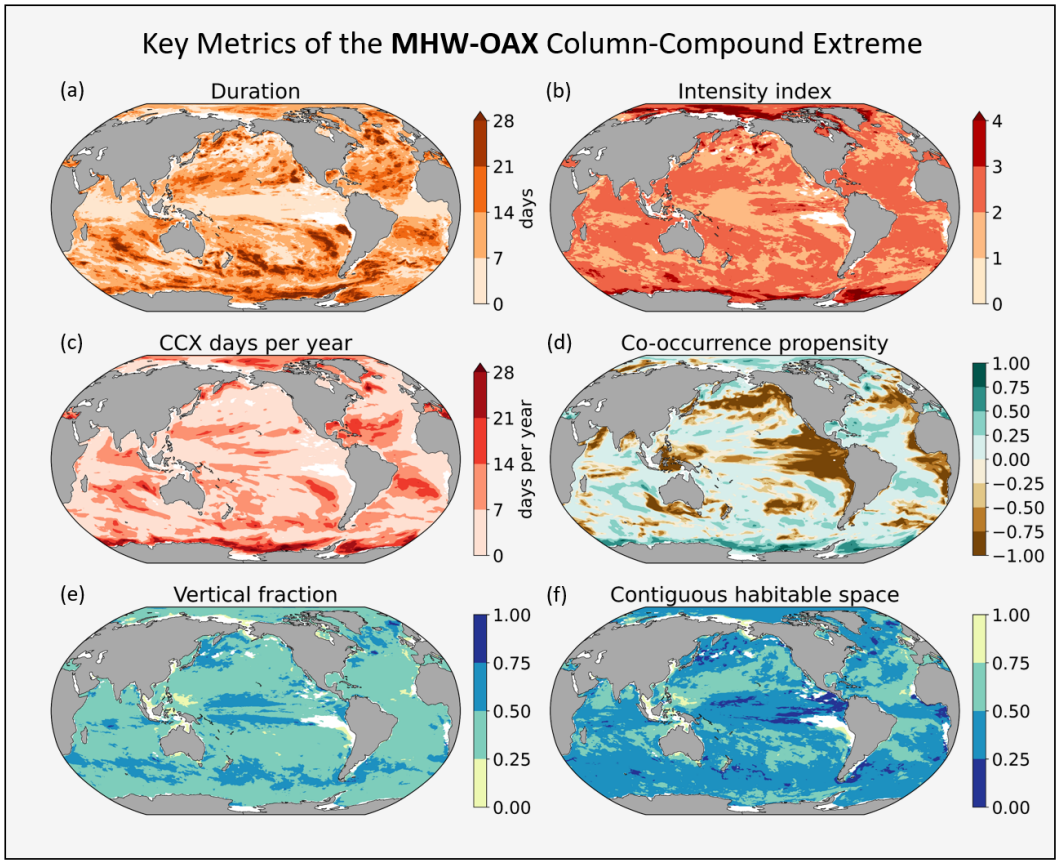

Figure 8. Key metrics of MHW-OAX events in the global ocean. (a) Mean duration, (b) mean annual maximum intensity index, (c) mean annual CCX days, (d) mean co-occurrence propensity, (e) mean fraction of water column occupied by extremes, and (f) mean fraction of contiguous habitable space in the vertical column

erage, and 81 % in area fraction of MHW-OAX events. In cluster 2, we see the strongest surface intensified signal, with MHW and OAX co-occuring at the same depths of 0 −100 m. The co-occurrence of MHW and OAX in the tropics and subtropics near the surface suggests that OAX is primarily induced by MHW, and is elucidated by Burger et al. (2022); Burger and Frölicher (2023), who detected surface MHW-OAX events in the same regions. Increases in temperature during MHWs directly lead to an increase in $[H^+]$ through shifts in the carbonate chemistry equilibrium. MHWs on the surface also increases stratification and reduces the mixing of deep, nutrient-rich waters. Biological productivity is suppressed, leading to an increase in DIC and thus $[H^+]$. In cluster 1, we observe a bimodal depth distribution of the MHW and OAX signals, with one at the surface similar to cluster 2, and a weaker distribution in the subsurface. This cluster occurs on the borders of the other clusters and act as a transition zone between them, as waters are being mixed and advected. Surface waters extreme in MHW-OAX may be horizontally advected through ocean currents (Holbrook et al., 2019; Sen Gupta et al., 2020; Elzahaby et al., 2021). Furthermore, downwelling Kelvin and Rossby waves propagate, maintain, and deepen the MHW-OAX signal (Holbrook et al., 2019; Zhang et al., 2021; Maulida et al., 2022; Qi et al., 2022). Surface and subsurface waters extreme with MHW and OAX may mix horizontally, forming the depth distribution seen in cluster 1.

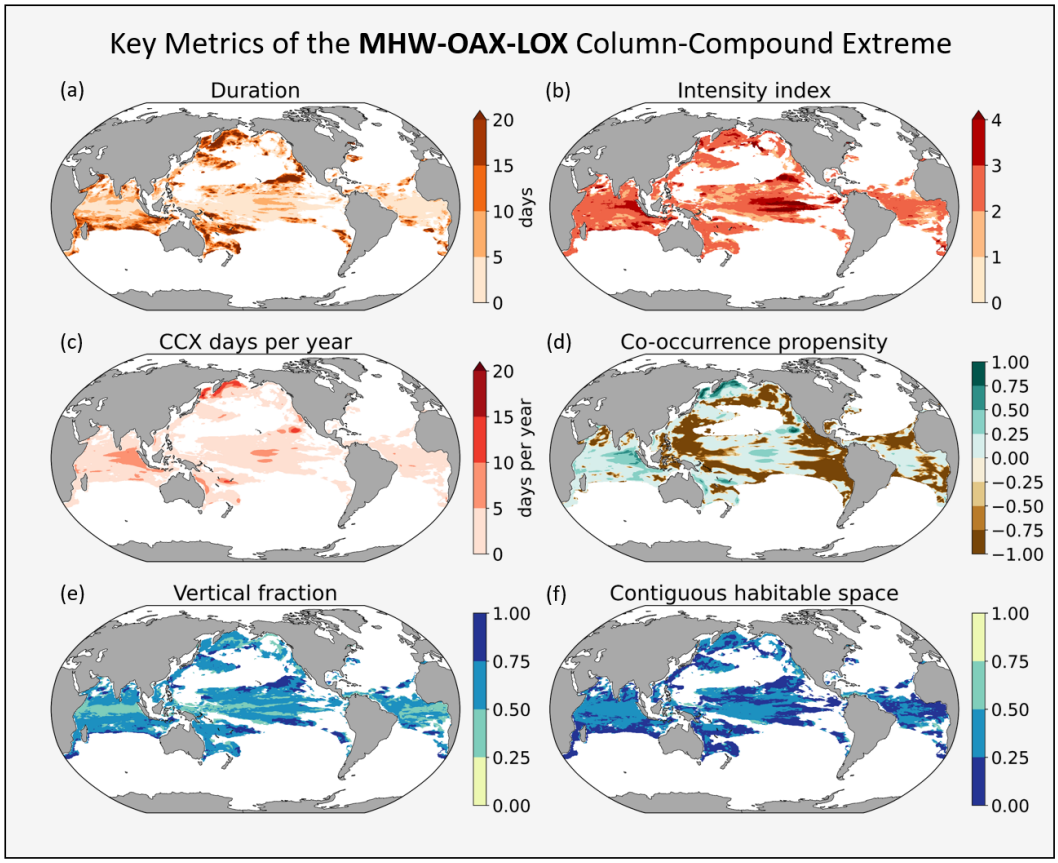

Figure 9. As Figure 8, but for triple compound events.

In clusters 3 and 4 we see the opposite, with MHW and OAX co-occurring in the subsurface. In cluster 3, we observe MHW intensified beneath the surface between 50 −300 m, with OAX occurring in the lower half of the water column below 100 m. The spread across the water column causes this cluster to have the highest vertical fraction of 46 %. Much of the cluster lies in the Subantarctic zone, within the Antarctic Circumpolar Current (ACC). In particular, the Scotia Sea, Drake Passage, and Macquarie Ridge stand out as regions with enhanced diapycncal mixing (Ledwell et al., 2011). Strong wind-driven currents and rough bathymetry may mix surface MHWs into the subsurface (Pellichero et al., 2017; Vogt et al., 2022). Local parcels of water carrying the MHW signal may be disconnected from the surface, and later reconnected again through mixing and surface heating. Meanwhile, anomalous intensification of winds drive the upwelling of CO_2-rich waters within the ACC and Antarctic convergence zone (Negrete-García et al., 2019; Ramadhan et al., 2022), heaving the thermocline and hence also waters with higher acidity, inducing OAX in the subsurface. The events of cluster 4 occur along the continent of Antarctica, with co-located MHW and OAX occurring largely beneath the surface between 100 −300 m. Here, MHW-OAX events have the highest frequency of 21 days per year, the longest mean duration of 19 days, and have the highest intensity index of 3.3. Strengthened zonal westerlies driving the Antarctic Circumpolar Current (ACC) could lead to increased upwelling of Circumpolar Deep Water (CDW) at the northern edge of the sea-ice zone (Morrison et al., 2015; Wilson et al., 2019; Ramadhan et al., 2022). This results in vertical entrainment of deep waters which tend to be warmer and more acidic (Gordon, 1981; Gordon & Huber, 1990; Pellichero et al., 2017). In periods of anomalously

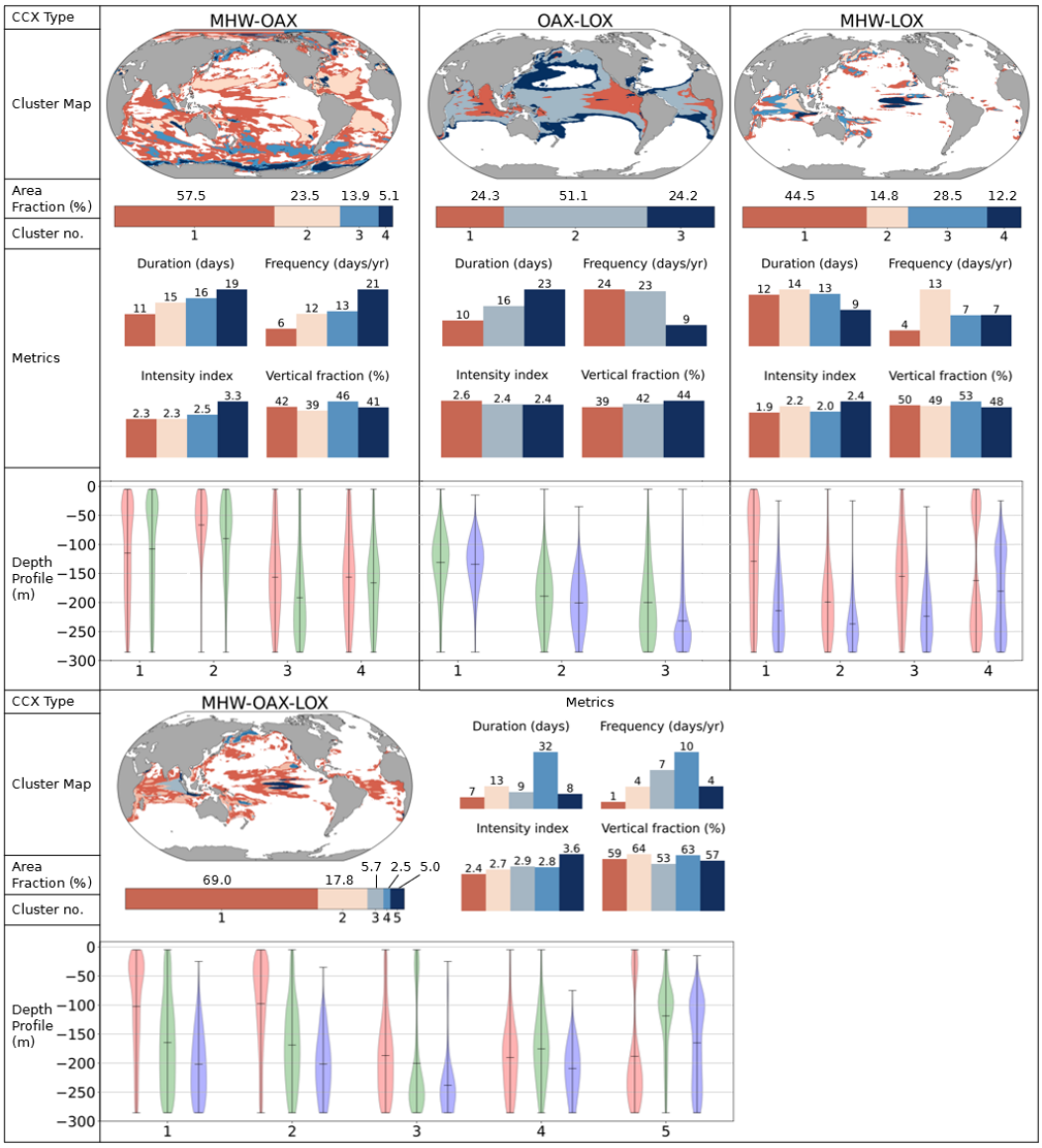

Figure 10. Summary of the main cluster characteristics identified by k-means clustering for each CCX type, i.e., MHW-LOX (top left column), OAX-LOX (top middle column), MHW-LOX (top right column), and the triple CCX MHW-OAX-LOX (bottom row). For each type, four groups of characteristics are provided (from the top): Horizontal distribution by a cluster map, cluster numbers and the area fraction occupied by each cluster as a horizontal bar plot, key metrics including cluster-averaged values of mean duration, mean days per year, mean annual column-maximum intensity index, and mean vertical fraction occupied by extremes as a vertical bar plots, and vertical distribution in the form of vertical violin plots. The latter show the sum of single grid-cell extreme occurrences during CCXs, weighted by their intensity index.

low sea ice extent, increased exposure of the surface to westerlies will also enhance upwelling of the CDW (Ramadhan et al., 2022).

OAX-LOX events are divided into three clusters (see Figure 10 middle column), where each cluster may be found in the same areas of each ocean basin. Cluster 1 roughly

corresponds to the eastern tropics and the Eastern Boundary Upwelling Systems (EBUS) regions, with OAX and LOX located together between 100 m and 300 m deep. Cluster 2 events are located higher in the water column, between 50 m and 200 m, and are located along the boundaries of cluster 1, reaching to the western side of the basins. Cluster 3 is located along the boundaries of the subtropical gyres, where the deepest events are found at below 100 m. The locations and depths of these clusters are reflective of the locations of oxygen minimum zones (OMZs), which are closest to the surface in the EBUS, eastern tropical Pacific, subarctic Pacific, and the Indian Ocean, deeper in the western tropics, and disappears towards the subtropical gyres (Gilly et al., 2013). This suggests that OAX-LOX events are caused by variability in the size, intensity, and vertical position of OMZs. The association of low pH and low oxygen in waters at depth is also well-known (Paulmier et al., 2011; Gobler & Baumann, 2016), so that OMZ variability can be linked to OAX-LOX events. Upwelling regions like the EBUS and equatorial regions are susceptible to the shoaling of the OMZ by anomalous wind-driven upwelling/thermocline heaving events (Espinoza-Morriberón et al., 2019; José et al., 2019; Turi et al., 2018; Köhn et al., 2022). Deep waters high in carbon and low in oxygen are upwelled, which manifests as a OAX-LOX signal. Anomalous upwelling is also identified in the Gulf of Alaska, driven by variable wind stress curl and depressed sea surface height in the subpolar gyre (Hauri et al., 2021). In the western tropical Pacific and tropical Indian ocean, OAX-LOX events likely also occur during a shoaling of the thermocline, so that the OMZ shifts laterally closer to the surface (Xu et al., 2017; Leung, Thompson, et al., 2019; G. Yang et al., 2019).

Due to the high spatial correlation between MHW-LOX and MHW-OAX-LOX events, their clusters are also analogous (contrast Figure 10 right column with bottom row). MHW-OAX-LOX cluster 5 (MHW-LOX cluster 4) is located in the central equatorial Pacific, is the most intense (3.6) of all CCX clusters, but has a relatively short duration (9 days) and low days per year (4 days per year). The triple compound cluster with the longest duration (32 days) and highest days per year (10 days per year) is found in the Bering sea of cluster 4 (MHW-LOX cluster 2). In the eastern tropical Indian ocean, we find MHW-OAX-LOX cluster 3 (MHW-LOX cluster 2) occurring 7 days per year. Finally, MHW-OAX-LOX clusters 1 and 2 (MHW-LOX clusters 1 and 3) occupies the largest area fraction of 86.8 %, and borders the other clusters in the tropics and North Pacific.

In MHW-OAX-LOX clusters 1 and 2, surface intensified extreme signals in temperature are clearly separated from the depth intensified signals in acidity and oxygen, as vertical entrainment and/or mixing is restricted across the thermocline. . Anomalous heating of the surface stratifies the surface layer and confines the MHW signal to the top $100-150$ m of the column. Meanwhile, OAX and LOX are intensified below the MHW during heaving or upwelling events. However, certain conditions allow heat to transfer below the thermocline leading to distinctive CCX depth profiles. The MHW-OAX-LOX cluster 5 in the central tropical Pacific is one such example, where MHW is intensified at the surface ($0-50$ m), and at depth ($150-300$ m). Meanwhile, OAX and LOX occupies the gap between $50-150$ m. During El Niño periods, strong anomalous surface heating takes place in the eastern tropical Pacific, deepening the thermocline and inducing MHWs throughout the water column (Fiedler & Lavín, 2017). On the western side of the Pacific the thermocline shoals, causing subsurface OAX and LOX extending into the central tropical Pacific (Xu et al., 2017; Leung, Thompson, et al., 2019). Thus the triple compound occurs when all three stressors occur in the same column, albeit at different vertical locations. When the surface heating tapers towards the end of El Niño, the MHW signal at the bottom of the column remains below the thermocline and is cut off from surface ventilation, leading to the characteristic depth profile seen in Figure 10. This subsurface MHW signal persists even into the succeeding La Niña event, where the shoaling thermocline in the east leads to intensified OAX and LOX above the MHW. This process is illustrated in the Hovmoller schematic of Figure 12, and through a video (Supporting Information Movie S1).

In the eastern tropical Indian ocean and the Bering sea, corresponding to MHW-OAX-LOX clusters 3 and 4, an unusual combination of all three stressors co-occur in the subsurface below 100 m with little to no surface-MHW expression. Unlike the Antarctic region, there is not any known deep water mass of higher temperature in these areas. One possible cause of MHW-OAX-LOX in cluster 4 is the Pacific Blob event in 2014-2016, which saw intense MHWs covering the northeastern Pacific, mixing into the subsurface and persisting below the mixed layer. Triple compound events of MHW, OAX, and LOX were also found in the water column during this time (Gruber et al., 2021). The warm water mass advected into the Bering Sea in 2017-2018 (Basyuk & Zuenko, 2020; Stabeno & Bell, 2019), and may be represented by a peak in MHW-OAX-LOX in 2018 (Supporting Information Figure S11). Subsequently, lower sea-ice cover in the winter led to anomalous stratification and reduced vertical mixing from melting ice (Stabeno & Bell, 2019; Scannell et al., 2020), prolonging the lifetime of the CCX in the subsurface. In cluster 3, the largest event occurred in 1997, corresponding with the largest event of cluster 5, and a strong El Niño event (Supporting Information S11). This suggests an ENSO teleconnection in the Indian ocean leading to subsurface MHW-OAX-LOX. In these two clusters, few MHW studies have been done, and even less so on subsurface MHW, OAX, and LOX. As research in this space has been gradually gaining attention, we expect to better understand the mechanisms behind these subsurface triple compound events in the future.

4.5 Enhancement and Suppression of CCXs during ENSO Events

Further insights into the potential drivers of CCX can be deduced from when the CCX occur. We have already seen that at the global scale, most CCX tend to correlate positively with ENSO (Figure 6). But we also identified more complex responses with enhanced occurrences during both strong El Niños and strong La Niñas. Thus, it is well warranted to examine this connection in depth, looking at the regional changes in CCX days during El Niño (Figure 11a,c,e,g) and La Niña (Figure 11b,d,f,h) events.

During ENSO events, there is an enhancement of all MHW-related CCXs in the tropics across all basins, up to 10 days per year in many areas (Figures 11a-b,e-f,g-h). There are clear spatial differences between the opposite phases of ENSO for MHW-OAX (Figures 11a-b). In general, El Niño does not suppress MHW-OAX strongly in any location, but instead enhances it in the tropics and subtropics of all ocean basins by about 20 days per year on average. There is particularly strong enhancement of up to 30 days per year in the Atlantic ocean and Arabian sea, which can be attributed to teleconnections with ENSO (Holbrook et al., 2019; Sen Gupta et al., 2020; Chatterjee et al., 2022). During La Niña, surface MHW-OAX may be observed in the typical chevron pattern of the western subtropical Pacific (Holbrook et al., 2019). The regions highlighted belong to MHW-OAX clusters 1 and 2, both of which have a strong surface expression. There are also more distinct features across the globe during La Niña. Notably, there are confined regions of strong enhancement and suppression in the Subantarctic and Antarctic zones, and mostly fall within MHW-OAX clusters 3 and 4. These clusters have a stronger subsurface expression, but the same regions can be identified in Holbrook et al. (2019) linking surface MHW to various climate modes. In these regions, modes such as the southern annular mode (SAM) likely drive variability in surface wind stress, leading to changes in the depth of the thermocline and hence subsurface extremes.

With MHW-LOX and MHW-OAX-LOX, there are no distinct spatial differences between the positive and negative phases of ENSO, with the exception of the central equatorial Pacific. Here, there is a strong increase in annual CCX days during El Niño by up to 30 days per year. This corresponds to cluster 5 of the triple compound event, which has most distinctive peak in volume fraction in the El Niño years of 1997 and 2016 (Supporting Information Figure S11). Both the surface MHW from the east and the subsurface OAX and LOX from the west trace their driver to El Niño, thus having a single com-

mon driver, though operating through different processes in different sides of the tropical Pacific. The lack of a strong ENSO correlation in the eastern tropical Pacific is different from the results of Holbrook et al. (2019); Sen Gupta et al. (2020) where there is a strong response in the eastern equatorial Pacific. This was also reflected in the co-occurrence propensities of MHW-related CCXs (Figure 7. MHWs induced on the surface during El Niño strongly stratify the surface, suppressing the upwelling of deep waters and hence reducing the occurrence of OAX and LOX. While some surface MHWs induce co-located OAX, the variability of $[H^+]$ due to this temperature effect is lower than that of upwelled low carbon waters during other periods such as La Niña, and is hence not detected as extreme within the 95th percentile.

Among the CCX variations, OAX-LOX events stand out as having the most distinct ENSO associations 11c-d) in both spatial distribution and magnitude. In the tropical Pacific, the opposing effects of El Niño and La Niña phases are clear. During El Niño, OAX-LOX events are enhanced in the west by more than 30 days (cluster 2), representing a doubling in annual CCX days. Meanwhile, a strong suppression of up to 30 days is observed in the eastern tropical Pacific (cluster 1). Conversely during La Niña, the eastern tropical Pacific (cluster 1) experiences an enhancement of OAX-LOX of a similar magnitude, and a weaker suppression in the west (cluster 2). These events can be strongly linked to ENSO with the shoaling and deepening of the thermocline, as highlighted in the previous section. ENSO effects on OAX-LOX in other regions are also strong, though not as distinctly dichotomous between phases. They are typically facilitated by atmospheric teleconnections (Roy & Reason, 2001) and ocean currents (Susanto et al., 2001; Feng et al., 2018), through mechanisms such as thermocline and upwelling modulations.

5 Discussion

Most studies on marine extremes have focused so far on surface MHWs, permitting scientists to limit their analyses to the drivers and impacts occurring in the surface layer. With the CCXs detected in this study, there is a need to infer surface and subsurface drivers. Moreover, CCXs in this study with surface expressions extend at least 50 m into the subsurface, prompting an investigation of surface stratification and the mixed layer. Similarly, the associated impacts of CCXs are relevant not just to organisms residing at a certain depth, but also to those who inhabit the entire water column. These migrating organisms are impacted to a greater extent as CCXs shrink and divide their habitable space.

5.1 Drivers of Column-Compound Extreme Events

The most significant CCX clusters identified in Section 4 are summarised in Figure 12, with their corresponding metrics and vertical structure. Within these clusters, we find that CCXs tend to occur at similar depths, suggesting similar drivers. With the analysis we have also repeatedly identified ENSO events as the main driver of large proportion of CCXs. This is due to the large area of the Pacific ocean typically affected by ENSO, and the atmospheric and oceanic connections it has with other ocean basins. However, the mechanisms through which ENSO drives CCX varies with region. Furthermore, ENSO events can drive CCXs through multiple mechanisms.

Some of these ENSO-driven CCXs have been identified as being spatially co-occurring, where their constituent single extremes co-occur in the same grid cells and tend to driven by similar mechanisms. The most prominent example is OAX-LOX, which primarily occurs in the subsurface. The OAX-LOX clusters 1 and 2 exhibit this effect at different depths, which are dependent on the location of the thermocline. La Niña events associated with an increase in surface winds drive anomalous upwelling of low-pH and low-oxygen waters in California and Humboldt current systems, leading to events in the OAX-

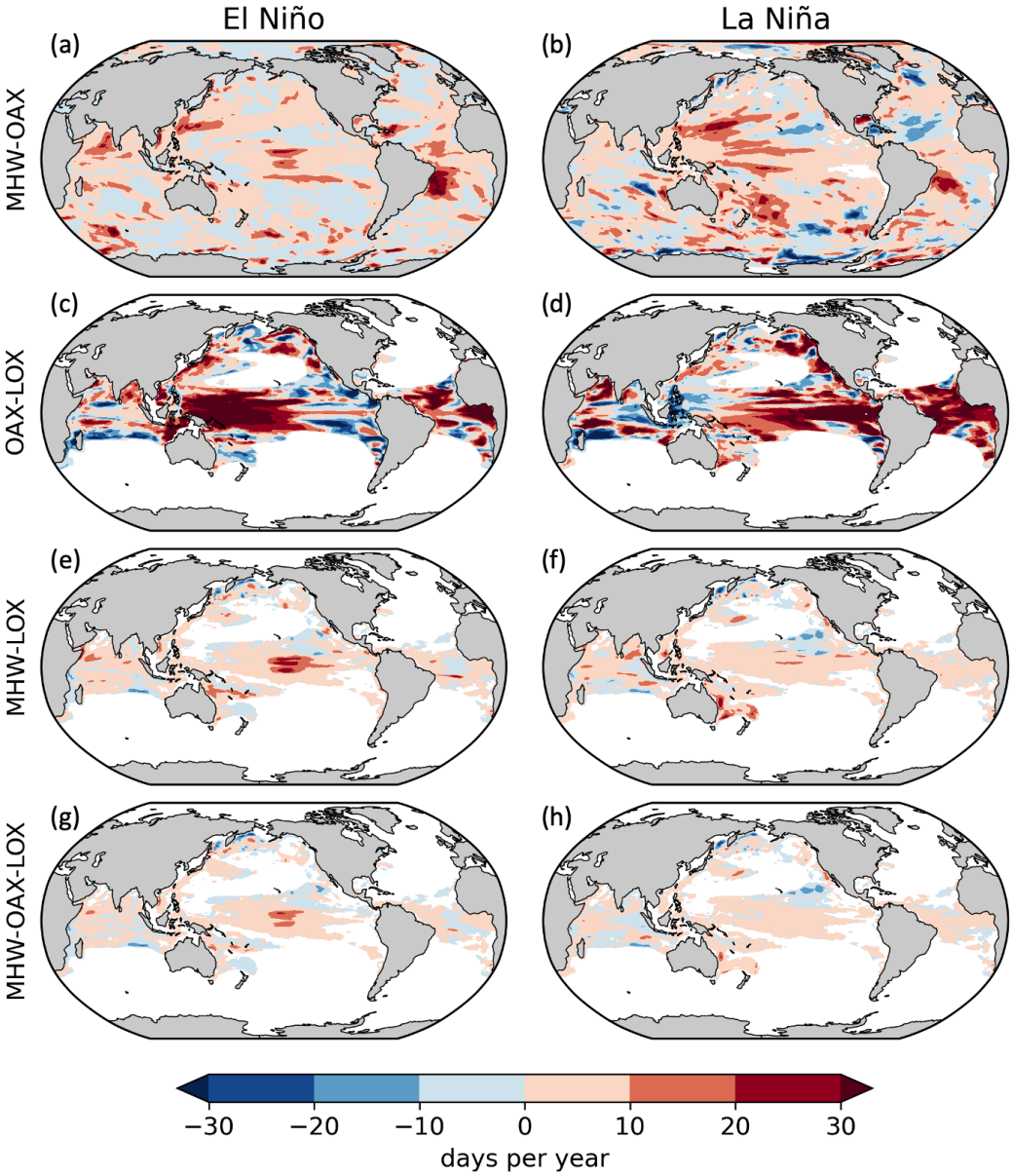

Figure 11. Maps illustrating the impact of ENSO on the number of extreme days for each CCX type. Shown are changes of annual CCX days during positive (left column) and negative (right column) ENSO phases, compared to a neutral ENSO phase. Each row corresponds to one CCX type, i.e. (a-b): MHW-OAX, (c-d): OAX-LOX, (e-f): MHW-LOX, (g-h): MHW-OAX-LOX. In this figure, a year is defined to begin in July and end in June of the next year, permitting to better capture the impact of ENSO as it peaks around Christmas.

LOX 1 cluster. Furthermore, the enhanced biological productivity induced by the upwelled waters further depletes oxygen through remineralisation. The depth of OAX and LOX during OAX-LOX events in the EBUS regions and east tropics cluster lies between 50 −200 m, which corroborates with the typical coastal and offshore upwelling source waters of 150 −280 m (Chhak & Di Lorenzo, 2007; Frischknecht et al., 2018; Bograd et al., 2015), and sits beneath the mean mixed layer depth (Ando & McPhaden, 1997; Fiedler

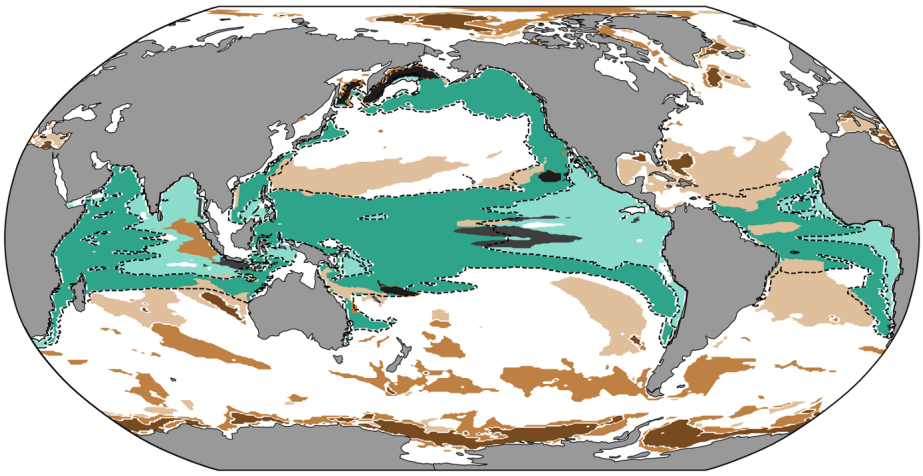

Cluster	MHW-OAX 2	MHW-OAX 3	MHW-OAX 4	OAX-LOX 1	OAX-LOX 2	MHW-OAX-LOX 5	MHW-OAX-LOX 4
Associated Regions	Subtropics, Tropics	Subantarctic	Antarctic	EBUS, East tropics	West tropics, OMZs	Central Tropical Pacific	Western Subarctic Pacific
Hovmoller Schematic							
Duration (days)	15 (49)	16 (40)	19 (29)	10 (27)	16 (39)	8 (13)	32 (52)
Frequency (days per year)	12 (81)	13 (58)	21 (50)	24 (67)	23 (53)	4 (16)	10 (20)
Intensity Index	2.3 (11.5)	2.5 (9.7)	3.3 (7.8)	2.6 (5.6)	2.4 (5.9)	3.6 (5.4)	2.8 (4.5)
Vertical Extent (%)	39 (88)	46 (83)	41 (79)	39 (70)	42 (75)	57 (75)	63 (81)
ENSO (+/-) change (days)	+2/+2	0/+2	-8/-5	+3/+13	+11/+8	+5/+3	-3/-5

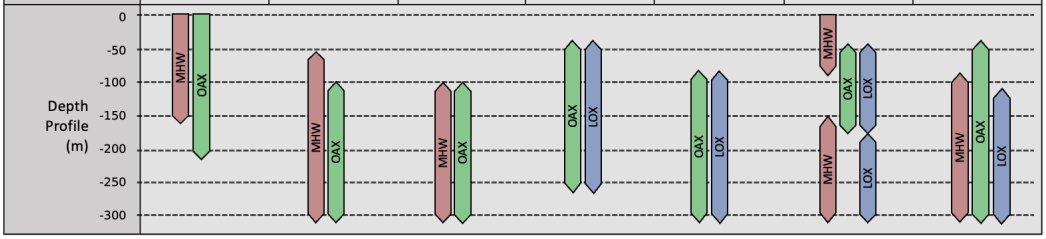

Figure 12. Synthesis figure of CCX properties in selected clusters. Map: Selected clusters of CCXs in a composite plot. The extent of OAX-LOX 1 and OAX-LOX 2 are marked by dashed lines to indicate their overlap with other clusters. Table (from top to bottom): Cluster names and their associated regions. Hovmoller schematics that are drawn to illustrate actual extreme conditions seen in the hindcast. Cluster mean values of mean duration, mean frequency, mean intensity index, mean vertical extent, and change in number of CCX days during positive and negative ENSO periods. Values in brackets are of the fixed baseline. Lastly, the approximate vertical locations of single extremes during CCXs are represented with simplified bars.

& Talley, 2006). Furthermore, the shoaling of the thermocline in the east tropics intensifies OAX and LOX in the subsurface. The co-occurrence propensity and vertical location of these events correspond roughly with the locations of low oxygen zones or shadow zones (Luyten et al., 1983; Paulmier & Ruiz-Pino, 2009), which are often associated with low pH (Paulmier et al., 2011). In the western tropical Pacific corresponding to OAX-LOX cluster 2, El Niño events lead to the shoaling of the thermocline, bringing low pH

and low oxygen waters closer to the surface, with mean depths corresponding to the mean mixed layer depth (Ando & McPhaden, 1997; Fiedler & Talley, 2006). In general, these events are deeper in the column than their eastern counterparts due to the deeper mixed layer depths in the western tropical Pacific. These events have the highest days per year among the identified clusters, increasing by the most during ENSO events. Another example of spatially co-occurring CCXs driven by ENSO is MHW-OAX cluster 2, predominantly in the subtropics. ENSO-driven temperature anomalies lead to MHWs (Holbrook et al., 2019), which then induces OAX through shifts in the carbonate chemistry equilibrium (Zeebe & Wolf-Gladrow, 2001; Burger et al., 2022).

ENSO events can also drive CCXs though multiple mechanisms, as seen in MHW-OAX-LOX cluster 5. MHW is induced throughout the column by strong surface heating during El Niño in the eastern tropical Pacific. Meanwhile, El Ni no also drives the shoaling of the thermocline in western tropical Pacific, inducing OAX and LOX in the subsurface. A deep MHW also persists in the subsurface even after being disconnected from the surface MHW. The resultant CCX is one which occupies the entire water column, driven by El Niño through different mechanisms. The MHW-OAX-LOX cluster 4 is another peculiar example, of which one occurrence in 2018 has been linked an El Niño event in 2014-2016 (Basyuk & Zuenko, 2020). Lateral advection of a warm water mass, enhanced southerly winds, and lower sea ice cover lead to the anomalous conditions in the Bering sea. The cluster has a low average association with ENSO, since our analysis does not account for lag times.

The CCXs in the Southern Ocean (MHW-OAX clusters 3 and 4) could be driven by various climate modes. Within these clusters, strong sub-cluster enhancements and suppression have been found during ENSO events, especially La Niña. Due to the varied ENSO response within the clusters, the cluster-mean change in days per year due to ENSO is rather muted. These CCXs have been found to be driven by a combination of surface heating, strong winds causing diapycnal mixing (Ledwell et al., 2011; Tamsitt et al., 2017), anomalous sea-ice cover (Ramadhan et al., 2022; Gordon, 1981), and upwelling along the Antarctic divergence zone (Morrison et al., 2015; Wilson et al., 2019; Ramadhan et al., 2022). These mechanisms can be linked to climate modes such as ENSO, SAM, IOD, and others.

5.2 Potential Impacts of Column-Compound Extreme Events

In this study we have identified a majority of CCXs occurring in the tropics and subtropics. The tropical nature of many CCXs is of particular concern given the fact that these regions are the harbinger of the highest diversity across nearly all trophic levels, ranging from phytoplankton (Righetti et al., 2019), zooplankton (Benedetti et al., 2021), fish (Stuart-Smith et al., 2013), to top predators (Worm & Tittensor, 2018). Also, the frequent occurrence of very intense MHW-OAX events in the high latitude Southern Ocean hits a very sensitive ecosystem, with a relatively high diversity (Chown et al., 2015).

Compounded extreme events are able to cause severe impacts when the stressors interact synergistically (Gruber et al., 2021). This synergism can happen in different ways. The most direct effects occur when an organism experiences multiple stressors in the same place and time (Le Grix et al., 2021; Burger et al., 2022). In our study, we additionally consider the contraction of habitable space within the water column during CCXs, where extremes may be occurring at different depths. This contraction may lead to indirect impacts related to predator evasion or food availability.

Co-located, co-temporal events exacerbate impacts on organisms to which multiple stressors are synergistically detrimental, and is highly dependent on the species and life stage (Kroeker et al., 2013; Deutsch et al., 2015; Gobler & Baumann, 2016). During compounded MHW and LOX, thermal stress increases metabolism and drives additional oxygen demand in ectotherms (Pörtner, 2002; K. E. Smith et al., 2023). The co-

inciding low oxygen environment further hinders the organisms' ability to survive, grow, or recruit. Recent works have quantified this effect into a composite "metabolic" or "aerobic growth" index (Deutsch et al., 2015; Clarke et al., 2021). MHWs and LOX occurring in the same place and time will pose a large threat in this case, albeit shown to be relatively uncommon in this work. However, a strong MHW can simultaneously induce lower oxygen (due to lower solubility), and reduce the low oxygen tolerance threshold of the organism (through increased metabolism), effectively increasing the oxygen threshold beyond those used in this study. Furthermore, acidic conditions have been shown to increase metabolic stress (Pan et al., 2015; Engström-Öst et al., 2019; Tai et al., 2021; Lattuca et al., 2023). Thus the co-occurrence of OAX adds another layer of metabolic demand. Every organism has a different metabolic threshold (Deutsch et al., 2015), and it is beyond the range of this study to identify impacts on any particular species. However, higher resolution regional studies (Franco et al., 2022) in conjunction with laboratory studies (Seibel et al., 2016) will be able to identify the impacts on metabolism of any given species.

Up until now, there is very little work on the compression of marine habitats due to extreme events (Desmet et al., 2022; Köhn et al., 2022), and much less so with compounded extreme stressors. In this study we show that when CCXs occur, the remaining continuous habitable space is less than half of the water column on average. This fraction reduces further when multiple extremes occur in different parts of the water column. Vertically migrating organisms are expected to be especially impacted by CCXs, since they depend on the habitable water column for essential biological activities. Diel vertical migration (DVM) is understood to be performed by planktonic species for the purpose of food gathering and predator avoidance (Ritz et al., 2011), and is a behavioural response to light (Cohen & Forward, 2019). Little is known about the impact of marine extremes on DVM, except that some species regularly migrate into low oxygen and low pH environments (Riquelme-Bugueño et al., 2020). When extreme conditions occurs close to the surface, the habitable space of migrating organisms is reduced. They may avoid the extreme conditions on the surface, thereby reducing food availability, or simply continue to migrate upwards into extreme conditions, increasing metabolism and food demand. In either case, ability of the organisms to grow and survive is reduced. In the event of a CCX that covers both the surface and subsurface, the migrating organisms have no good choice to make, and are simply subject to extreme conditions where ever they are. Habitat contraction may further impact organisms in more indirect ways. Extreme conditions on the surface may force marine fish to migrate into the subsurface (Jorda et al., 2020), decreasing the survivability of zooplankton species which use the darker environment to avoid predators.

5.3 Caveats and Limitations

Owing to the lack of data, the model results were evaluated with respect to surface MHWs and OAXs only, leaving us largely blind with regard to potential biases of the important processes at depth causing CCX. The evaluation of the surface OAX with OceanSODA-ETHZ (Gregor & Gruber, 2021) showed a tendency of the model towards longer and more intense events on the surface. Since this bias is located in the upwelling regions, we also expect it to apply to detected LOXs, due to their high co-occurrence in these regions. Overall, we expect the impact of potential biases on our results to be restricted to particular metrics, perhaps most importantly the intensity and duration of the events. In contrast, the spatial structure of the CCX and their co-occurence propensity is likely much less affected, as this is a result of large-scale processes, which we consider well captured by the model. One option for the subsurface evaluation of these properties is emerging from the rapidly increasing number of observations from the Biogeochemical Argo float program (Johnson & Claustre, 2016). These observations could be used to evaluate $[H^+]$ and $[O_2]$ in the subsurface, though their 10 day repeat cycle and wide spacing will require quite some effort to arrive at a robust extreme product.

A second caveat concerns the relatively low resolution of the atmospheric forcing employed in our CESM hindcast. This low resolution of the forcing affects atmosphere-forced extreme events, while ocean-forced events are likely much less affected. In the case of the former, long duration events, such as those associated with ENSO, are better represented compared to short duration events. In the case of ocean-forced events, e.g., through heaving and shoaling of the thermocline, we expect little impact of our choice. But still, and especially also when considering the moderate resolution of our model, our results are biased toward the longer-lasting CCXs extending over of substantial spatial scales.

The third caveat concerns the choice of criteria used to identify extremes. Our choices were made with the intention to investigate the co-occurrence of multiple stressors within the vertical column in a systematic and consistent manner, linking them to drivers and mechanisms based on their spatiotemporal characteristics. For this work, the moving baseline was primarily used, since it a better choice in the investigation of drivers behind extreme events. However in Figures 5 and 6 it was shown that the detected volume fraction is vastly different between that of the fixed and moving baselines. The results on the moving baseline are unable to show the worsening conditions of global ocean under climate change, nor the change in propensity of extreme events under such conditions. For such an analysis, the fixed baseline may be a better choice.

Furthermore, the chosen extreme criteria are not targeted towards specific biological thresholds or marine organisms. Thus, the impacts of the extremes identified in this study cannot be directly quantified. For example, MHW-OAX CCXs are generally absent in the EBUS, even though temperature-induced OAXs are known to occur during MHWs. This is likely because the OAX occurrences in these regions are dominated by anomalous upwelling events, which reduce pH more strongly compared to MHWs. Thus we see more OAX-LOX occurring in the EBUS. However, this does not mean that the MHW-induced low pH is irrelevant, as there may be organisms still affected. In such scenarios it is better to rely on species-specific thresholds as the basis of extreme detection. This limitation on biological impacts also extends to the definition of CCXs, where at least 50 m of each extreme type is required. An organism whose metabolism is affected by temperature could be affected by either MHWs or LOXs, and not necessarily only when both occur. It may then be a better choice to define extreme conditions based on the metabolic rate of the particular organism and oxygen concentration in the water.

6 Summary and Conclusions

With this work on CCX, we make the first step in characterising extremes that are compounded in the vertical water column. CCXs are detected in the global ocean on a CESM-BEC daily hindcast from 1961 to 2020. Key characteristics like frequency, duration, intensity, and reduction of habitable space are assessed, to determine the regions where CCXs are the most severe. These are the subtropics and Southern ocean for MHW-OAX, and the tropics and north Pacific for OAX-LOX, MHW-LOX, and MHW-OAX-LOX. All CCX substantially increase in their intensity, frequency, and spatial extent, primarily driven by ocean warming and the increase in the ocean's acidity owing to the oceanic uptake of anthropogenic CO_2 from the atmosphere.

Within the vertical column, the depths where single extremes occur during CCXs are analysed to determine the mechanisms behind them. We find that ENSO-associated CCXs tend to be driven by a single mechanism such as increased air-sea heat flux or increased upwelling, resulting in co-located compounded events. On the other hand, there is a significant proportion of CCXs where the constituent single extremes occur in different parts of the vertical column. These tend to be driven by separate drivers, and have a reduced association with ENSO events.

Marine extreme events can have a large impact on pelagic organisms, which are usually affected by multiple, rather than a single stressor. These organisms swim or migrate vertically, experiencing various physical and chemical conditions. The study of vertically compounded extremes thus advances our understanding of the impacts of extreme events on marine organisms. Furthermore, these extremes are likely to become more frequent and intense with the climate trend of increasing temperatures and atmospheric CO_2. Extreme conditions of the past may well become the mean state of the ocean in the future. Further analysis of such column-compound events in regional scales or to with regard to specific organisms will extend our understanding of their future impacts.

Open Research

All data to reproduce the plots can be found under the following repository: `https://doi.org/10.3929/ethz-b-000626173`. Model output data may be obtained upon request from the corresponding author (joel.wong@usys.ethz.ch).

Conflict of Interest Statement

The authors have no conflicts of interest to declare.

Acknowledgments

This project has received funding from the European Union's Horizon 2020 research and innovation programme under grant agreement No 820989 (COMFORT). The authors thank Dr. Damian Loher for his modeling support, and Dr. Eike Köhn, Dr. Luke Gregor, and Dr. Fabio Benedetti for useful discussions.

References

Ando, K., & McPhaden, M. J. (1997). Variability of surface layer hydrography in the tropical Pacific Ocean. *Journal of Geophysical Research: Oceans*, *102*(C10), 23063–23078. doi: 10.1029/97JC01443

Basyuk, E., & Zuenko, Y. (2020). Extreme oceanographic conditions in the northwestern Bering Sea in 2017–2018. *Deep-Sea Research Part II: Topical Studies in Oceanography*, *181-182*. doi: 10.1016/j.dsr2.2020.104909

Bednaršek, N., Feely, R. A., Beck, M. W., Glippa, O., Kanerva, M., & Engström-Öst, J. (2018). El Niño-related thermal stress coupled with upwelling-related ocean acidification negatively impacts cellular to population-level responses in pteropods along the California current system with implications for increased bioenergetic costs. *Frontiers in Marine Science*, *5*, 1–17. doi: 10.3389/fmars.2018.00486

Benedetti, F., Vogt, M., Elizondo, U. H., Righetti, D., Zimmermann, N. E., & Gruber, N. (2021). Major restructuring of marine plankton assemblages under global warming. *Nature Communications*, *12*(1), 5226. doi: 10.1038/s41467-021-25385-x

Bertrand, A., Ballón, M., & Chaigneau, A. (2010). Acoustic observation of living organisms reveals the upper limit of the oxygen minimum zone. *PLoS ONE*, *5*(4). doi: 10.1371/journal.pone.0010330

Bianchi, D., & Mislan, K. A. (2016). Global patterns of diel vertical migration times and velocities from acoustic data. *Limnology and Oceanography*, *61*(1), 353–364. doi: 10.1002/lno.10219

Bianchi, D., Stock, C., Galbraith, E. D., & Sarmiento, J. L. (2013). Diel vertical migration: Ecological controls and impacts on the biological pump in a one-dimensional ocean model. *Global Biogeochemical Cycles*, *27*(2), 478–491. doi: 10.1002/gbc.20031

Bograd, S. J., Buil, M. P., Lorenzo, E. D., Castro, C. G., Schroeder, I. D., Goericke, R., ... Whitney, F. A. (2015). Changes in source waters to the Southern California Bight. *Deep-Sea Research Part II: Topical Studies in Oceanography*, *112*, 42–52. doi: 10.1016/j.dsr2.2014.04.009

Boyd, P. W., & Brown, C. J. (2015). Modes of interactions between environmental drivers and marine biota. *Frontiers in Marine Science*, *2*, 1–7. doi: 10.3389/fmars.2015.00009

Braun, C. D., Kaplan, M. B., Horodysky, A. Z., & Llopiz, J. K. (2015). Satellite telemetry reveals physical processes driving billfish behavior. *Animal Biotelemetry*, *3*(1). doi: 10.1186/s40317-014-0020-9

Burger, F. A., & Frölicher, T. L. (2023). Drivers of Surface Ocean Acidity Extremes in an Earth System Model. *Global Biogeochemical Cycles*, *37*(9), e2023GB007785. (Burger2023) doi: 10.1029/2023GB007785

Burger, F. A., John, J. G., & Frölicher, T. L. (2020). Increase in ocean acidity variability and extremes under increasing atmospheric CO_2. *Biogeosciences*, *17*(18), 4633–4662. doi: 10.5194/bg-17-4633-2020

Burger, F. A., Terhaar, J., & Frölicher, T. L. (2022). Compound marine heatwaves and ocean acidity extremes. *Nature Communications*, 1–12. doi: 10.1038/s41467-022-32120-7

Chan, F., Barth, J. A., Lubchenco, J., Kirincich, A., Weeks, H., Peterson, W. T., & Menge, B. A. (2008). Emergence of anoxia in the California current large marine ecosystem. *Science*, *319*(5865), 920. doi: 10.1126/science.1149016

Chatterjee, A., Anil, G., & Shenoy, L. R. (2022). Marine heatwaves in the Arabian Sea. *Ocean Science*, *18*(3), 639–657. doi: 10.5194/os-18-639-2022

Chhak, K., & Di Lorenzo, E. (2007). Decadal variations in the California Current upwelling cells. *Geophysical Research Letters*, *34*(14), 1–6. doi: 10.1029/2007GL030203

Chiswell, S. M. (2022). Global Trends in Marine Heatwaves and Cold Spells: The Impacts of Fixed Versus Changing Baselines. *Journal of Geophysical Research: Oceans*, *127*(10), e2022JC018757. doi: 10.1029/2022JC018757

Chown, S. L., Clarke, A., Fraser, C. I., Cary, S. C., Moon, K. L., & McGeoch, M. A. (2015). The changing form of Antarctic biodiversity. *Nature*, *522*(7557), 431–438. doi: 10.1038/nature14505

Clarke, T. M., Wabnitz, C. C., Striegel, S., Frölicher, T. L., Reygondeau, G., & Cheung, W. W. (2021). Aerobic growth index (AGI): An index to understand the impacts of ocean warming and deoxygenation on global marine fisheries resources. *Progress in Oceanography*, *195*. doi: 10.1016/j.pocean.2021.102588

Cohen, J. H., & Forward, R. B. (2019). Vertical Migration of Aquatic Animals. In J. C. Choe (Ed.), *Encyclopedia of Animal Behavior (Second Edition)* (pp. 546–552). Oxford: Academic Press. doi: 10.1016/B978-0-12-809633-8.01257-7

Collins, M., Sutherland, M., Bouwer, L., Cheong, S.-M., Frölicher, T., Des Combes, H. J., ... Tibig, L. (2019). *Extremes, Abrupt Changes and Managing Risks* (Tech. Rep.).

Crain, C. M., Kroeker, K., & Halpern, B. S. (2008). Interactive and cumulative effects of multiple human stressors in marine systems. *Ecology Letters*, *11*(12), 1304–1315. doi: 10.1111/j.1461-0248.2008.01253.x

Desmet, F., Gruber, N., Köhn, E. E., Münnich, M., & Vogt, M. (2022). Tracking the space-time evolution of ocean acidification extremes in the California Current System and Northeast Pacific. *Journal of Geophysical Research: Oceans*, 1–30. doi: 10.1029/2021jc018159

Desmet, F., Münnich, M., & Gruber, N. (2023). *Spatiotemporal heterogeneity in the increase of ocean acidity extremes in the Northeast Pacific.* doi: 10.5194/bg-2023-60

Deutsch, C., Ferrel, A., Seibel, B., Pörtner, H.-O., & Huey, R. B. (2015). Climate change tightens a metabolic constraint on marine habitats. *Science*, *348*(6239), 1132–1136. doi: DOI:10.1126/science.aaa1605

Diaz, R. J., & Rosenberg, R. (2008). Spreading Dead Zones and Consequences for Marine Ecosystems. *Science*, *321*(5891), 926–929. doi: 10.1126/science.1156401

Di Lorenzo, E., & Mantua, N. (2016). Multi-year persistence of the 2014/15 North Pacific marine heatwave. *Nature Climate Change*, *6*(11), 1042–1047. doi: 10.1038/nclimate3082

Ebita, A., Kobayashi, S., Ota, Y., Moriya, M., Kumabe, R., Onogi, K., ... Ishimizu, T. (2011). The Japanese 55-year Reanalysis "JRA-55": An Interim Report. *Sola*, *7*, 149–152. doi: 10.2151/sola.2011-038

Elzahaby, Y., Schaeffer, A., Roughan, M., & Delaux, S. (2021). Oceanic Circulation Drives the Deepest and Longest Marine Heatwaves in the East Australian Current System. *Geophysical Research Letters*, *48*(17), e2021GL094785. doi: 10.1029/2021GL094785

Engström-Öst, J., Glippa, O., Feely, R. A., Kanerva, M., Keister, J. E., Alin, S. R., ... Bednaršek, N. (2019). Eco-physiological responses of copepods and pteropods to ocean warming and acidification. *Scientific Reports*, *9*(1), 1–13. doi: 10.1038/s41598-019-41213-1

Espinoza-Morriberón, D., Echevin, V., Colas, F., Tam, J., Gutierrez, D., Graco, M., ... Quispe-Ccalluari, C. (2019). Oxygen variability during ENSO in the Tropical South Eastern Pacific. *Frontiers in Marine Science*, *5*, 1–20. doi: 10.3389/fmars.2018.00526

Feng, M., Zhang, N., Liu, Q., & Wijffels, S. (2018). The Indonesian throughflow, its variability and centennial change. *Geoscience Letters*, *5*(1), 3. doi: 10.1186/s40562-018-0102-2

Fiedler, P. C., & Lavín, M. F. (2017). Oceanographic Conditions of the Eastern Tropical Pacific. In P. W. Glynn, D. P. Manzello, & I. C. Enochs (Eds.),

Coral Reefs of the Eastern Tropical Pacific: Persistence and Loss in a Dynamic Environment (pp. 59–83). Dordrecht: Springer Netherlands. doi: 10.1007/978-94-017-7499-4_3

Fiedler, P. C., & Talley, L. D. (2006). Hydrography of the eastern tropical Pacific: A review. *Progress in Oceanography*, *69*(2-4), 143–180. doi: 10.1016/j.pocean.2006.03.008

Fragkopoulou, E., Sen Gupta, A., Costello, M. J., Wernberg, T., Araújo, M. B., Serrão, E. A., ... Assis, J. (2023, September). Marine biodiversity exposed to prolonged and intense subsurface heatwaves. *Nature Climate Change*, 1–8. doi: 10.1038/s41558-023-01790-6

Franco, A. C., Kim, H., Frenzel, H., Deutsch, C., Ianson, D., Sumaila, U. R., & Tortell, P. D. (2022). Impact of warming and deoxygenation on the habitat distribution of Pacific halibut in the Northeast Pacific. *Fisheries Oceanography*, *31*(6), 601–614. doi: 10.1111/fog.12610

Friedlingstein, P., Jones, M. W., Sullivan, M. O., Andrew, R. M., Bakker, D. C. E., Hauck, J., ... Peters, W. (2022). Global Carbon Budget 2021. *Earth System Science Data*, 1917–2005. doi: 10.5194/essd-14-4811-2022

Frischknecht, M., Münnich, M., & Gruber, N. (2018). Origin, Transformation, and Fate: The Three-Dimensional Biological Pump in the California Current System. *Journal of Geophysical Research: Oceans*, *123*(11), 7939–7962. doi: 10.1029/2018JC013934

Frölicher, T. L., Fischer, E. M., & Gruber, N. (2018). Marine heatwaves under global warming. *Nature*, *560*(7718), 360–364. doi: 10.1038/s41586-018-0383-9

Gent, P. R., Danabasoglu, G., Donner, L. J., Holland, M. M., Hunke, E. C., Jayne, S. R., ... Zhang, M. (2011). The Community Climate System Model Version 4. *Journal of Climate*, *24*(19), 4973–4991. doi: 10.1175/2011JCLI4083.1

Gilly, W. F., Michael Beman, J., Litvin, S. Y., & Robison, B. H. (2013). Oceanographic and biological effects of shoaling of the oxygen minimum zone. *Annual Review of Marine Science*, *5*, 393–420. doi: 10.1146/annurev-marine-120710-100849

Gleckler, P. J., Durack, P. J., Stouffer, R. J., Johnson, G. C., & Forest, C. E. (2016). Industrial-era global ocean heat uptake doubles in recent decades. *Nature Climate Change*, *6*(4), 394–398. doi: 10.1038/nclimate2915

Gobler, C. J., & Baumann, H. (2016). Hypoxia and acidification in ocean ecosystems: Coupled dynamics and effects on marine life. *Biology Letters*, *12*(5). doi: 10.1098/rsbl.2015.0976

Good, S., Embury, O., Bulgin, C., & Mittaz, J. (2019). *ESA Sea Surface Temperature Climate Change Initiative (SST_cci): Level 4 Analysis Climate Data Record, version 2.0.* Centre for Environmental Data Analysis (CEDA). doi: 10.5285/ACED40D7CB964F23A0FD3E85772F2D48

Good, S., Fiedler, E., Mao, C., Martin, M. J., Maycock, A., Reid, R., ... Worsfold, M. (2020). The Current Configuration of the OSTIA System for Operational Production of Foundation Sea Surface Temperature and Ice Concentration Analyses. *Remote Sensing*, *12*(4), 720. doi: 10.3390/rs12040720

Gordon, A. L. (1981). Seasonality of Southern Ocean Sea Ice. *Journal of Geophysical Research*, *86*(C5), 4193–4197. doi: 10.1029/JC086iC05p04193

Gordon, A. L., & Huber, B. A. (1990). Southern ocean winter mixed layer. *Journal of Geophysical Research*, *95*(C7), 11655. doi: 10.1029/jc095ic07p11655

Gregor, L., & Gruber, N. (2021). OceanSODA-ETHZ: A global gridded data set of the surface ocean carbonate system for seasonal to decadal studies of ocean acidification. *Earth System Science Data*, *13*(2), 777–808. doi: 10.5194/essd-13-777-2021

Gruber, N., Boyd, P. W., Frölicher, T. L., & Vogt, M. (2021). Ocean Biogeochemical Extremes and Compound Events. *Nature*, *600*, 395–407. doi: 10.1038/s41586-021-03981-7

Hauck, J., Zeising, M., Le Quéré, C., Gruber, N., Bakker, D. C. E., Bopp, L., ... Séférian, R. (2020). Consistency and Challenges in the Ocean Carbon Sink Estimate for the Global Carbon Budget. *Frontiers in Marine Science*, *7*.

Hauri, C., Gruber, N., McDonnell, A. M., & Vogt, M. (2013). The intensity, duration, and severity of low aragonite saturation state events on the California continental shelf. *Geophysical Research Letters*, *40*(13), 3424–3428. doi: 10.1002/grl.50618

Hauri, C., Pagès, R., McDonnell, A. M., Stuecker, M. F., Danielson, S. L., Hedstrom, K., ... Doney, S. C. (2021). Modulation of ocean acidification by decadal climate variability in the Gulf of Alaska. *Communications Earth and Environment*, *2*(1), 1–7. Retrieved from `http://dx.doi.org/10.1038/s43247-021-00254-z` doi: 10.1038/s43247-021-00254-z

Hobday, A. J., Alexander, L. V., Perkins, S. E., Smale, D. A., Straub, S. C., Oliver, E. C., ... Wernberg, T. (2016). A hierarchical approach to defining marine heatwaves. *Progress in Oceanography*, *141*, 227–238. doi: 10.1016/j.pocean.2015.12.014

Hobday, A. J., Oliver, E. C., Gupta, A. S., Benthuysen, J. A., Burrows, M. T., Donat, M. G., ... Smale, D. A. (2018). Categorizing and naming marine heatwaves. *Oceanography*, *31*(2), 162–173. doi: 10.5670/oceanog.2018.205

Hofmann, A. F., Peltzer, E. T., Walz, P. M., & Brewer, P. G. (2011). Hypoxia by degrees: Establishing definitions for a changing ocean. *Deep-Sea Research Part I: Oceanographic Research Papers*, *58*(12), 1212–1226. doi: 10.1016/j.dsr.2011.09.004

Holbrook, N. J., Claar, D. C., Hobday, A. J., McInnes, K. L., Oliver, E. C. J., Gupta, A. S., ... Zhang, X. (2020). ENSO-Driven Ocean Extremes and Their Ecosystem Impacts. *El Niño Southern Oscillation in a Changing Climate*, 409–428.

Holbrook, N. J., Scannell, H. A., Sen Gupta, A., Benthuysen, J. A., Feng, M., Oliver, E. C., ... Wernberg, T. (2019). A global assessment of marine heatwaves and their drivers. *Nature Communications*, *10*(1), 1–13. doi: 10.1038/s41467-019-10206-z

Holbrook, N. J., Sen Gupta, A., Oliver, E. C. J., Hobday, A. J., Benthuysen, J. A., Scannell, H. A., ... Wernberg, T. (2020). Keeping pace with marine heatwaves. *Nature Reviews Earth & Environment*, *1*(9), 482–493. doi: 10.1038/s43017-020-0068-4

Hunke, E., & Lipscomb, W. (2008). *CICE: The Los Alamos sea ice model documentation and software user's manual version 4.0* (Tech. Rep.). Los Alamos NM 87545: T-3 Fluid Dynamics Group, Los Alamos National Laboratory.

Jacox, M. G. (2019). Marine heatwaves in a changing climate. *Nature*, *571*(7766), 485–487. doi: 10.1038/d41586-019-02196-1

Johnson, K., & Claustre, H. (2016). The scientific rationale, design, and implementation plan for a Biogeochemical-Argo float array. *Biogeochemical-Argo Planning Group*. doi: 10.13155/46601

Jorda, G., Marbà, N., Bennett, S., Santana-Garcon, J., Agusti, S., & Duarte, C. M. (2020). Ocean warming compresses the three-dimensional habitat of marine life. *Nature Ecology and Evolution*, *4*(1), 109–114. doi: 10.1038/s41559-019-1058-0

José, Y. S., Stramma, L., Schmidtko, S., & Oschlies, A. (2019). ENSO-driven fluctuations in oxygen supply and vertical extent of oxygen-poor waters in the oxygen minimum zone of the Eastern Tropical South Pacific. *Biogeosciences Discussions*, 1–20.

Kroeker, K. J., Kordas, R. L., Crim, R., Hendriks, I. E., Ramajo, L., Singh, G. S., ... Gattuso, J. P. (2013). Impacts of ocean acidification on marine organisms: Quantifying sensitivities and interaction with warming. *Global Change Biology*, *19*(6), 1884–1896. doi: 10.1111/gcb.12179

Kwiatkowski, L., & Orr, J. C. (2018). Diverging seasonal extremes for ocean acidification during the twenty-first century. *Nature Climate Change*, *8*(2), 141–145. doi: 10.1038/s41558-017-0054-0

Kwiatkowski, L., Torres, O., Bopp, L., Aumont, O., Chamberlain, M., Christian, J. R., ... Ziehn, T. (2020). Twenty-first century ocean warming, acidification, deoxygenation, and upper-ocean nutrient and primary production decline from CMIP6 model projections. *Biogeosciences*, *17*(13), 3439–3470. doi: 10.5194/bg-17-3439-2020

Köhn, E. E., Münnich, M., Vogt, M., Desmet, F., & Gruber, N. (2022). Strong Habitat Compression by Extreme Shoaling Events of Hypoxic Waters in the Eastern Pacific. *Journal of Geophysical Research: Oceans*, *127*(6). doi: 10.1029/2022jc018429

Köhn, E. E., Vogt, M., Münnich, M., & Gruber, N. (2023). *On the vertical structure and propagation of marine heatwaves in the Eastern Pacific.* doi: 10.22541/essoar.168565400.06607545/v1

Lattuca, M. E., Vanella, F. A., Malanga, G., Rubel, M. D., Manríquez, P. H., Torres, R., ... Fernández, D. A. (2023). Ocean acidification and seasonal temperature extremes combine to impair the thermal physiology of a sub-Antarctic fish. *Science of the Total Environment*, *856*. doi: 10.1016/j.scitotenv.2022.159284

Ledwell, J. R., St. Laurent, L. C., Girton, J. B., & Toole, J. M. (2011). Diapycnal mixing in the antarctic circumpolar current. *Journal of Physical Oceanography*, *41*(1), 241–246. doi: 10.1175/2010JPO4557.1

Le Grix, N., Zscheischler, J., Laufkötter, C., Rousseaux, C. S., & Frölicher, T. L. (2021). Compound high-temperature and low-chlorophyll extremes in the ocean over the satellite period. *Biogeosciences*, *18*(6), 2119–2137. doi: 10.5194/bg-18-2119-2021

Le Grix, N., Zscheischler, J., Rodgers, K. B., Yamaguchi, R., & Frölicher, T. L. (2022). Hotspots and drivers of compound marine heatwaves and low net primary production extremes. *Biogeosciences*, *19*(24), 5807–5835. doi: 10.5194/bg-19-5807-2022

Leung, S., Mislan, K. A. S., Muhling, B., & Brill, R. (2019). The significance of ocean deoxygenation for open ocean tunas and billfishes. In *'Laffoley, D. & Baxter, J.M. (eds.) (2019). Ocean deoxygenation: Everyone's problem - Causes, impacts, consequences and solutions.* (pp. 277–308). IUCN, Gland, Switzerland. doi: 10.2305/IUCN.CH.2019.13.en

Leung, S., Thompson, L. A., McPhaden, M. J., & Mislan, K. A. (2019). ENSO drives near-surface oxygen and vertical habitat variability in the tropical Pacific. *Environmental Research Letters*, *14*(6). doi: 10.1088/1748-9326/ab1c13

Luo, J. J., Zhang, R., Behera, S. K., Masumoto, Y., Jin, F. F., Lukas, R., & Yamagata, T. (2010). Interaction between El Niño and extreme Indian Ocean dipole. *Journal of Climate*, *23*(3), 726–742. doi: 10.1175/2009JCLI3104.1

Luyten, R., J., Pedlosky, J., & Stommel, J. (1983). The Ventilated Thermocline. *Journal of Physical Oceanography*. doi: 10.1175/1520-0485(1983)013⟨0292:TVT⟩2.0.CO;2

Ma, D., Gregor, L., & Gruber, N. (2023). Four Decades of Trends and Drivers of Global Surface Ocean Acidification. *Global Biogeochemical Cycles*, *37*(7), e2023GB007765. doi: 10.1029/2023GB007765

MacQueen, J. (1967). Some methods for classification and analysis of multivariate observations. In *Proceedings of the fifth Berkeley symposium on mathematical statistics and probability* (Vol. 1, pp. 281–297). Oakland, CA, USA.

Marin, M., Feng, M., Bindoff, N. L., & Phillips, H. E. (2022). Local Drivers of Extreme Upper Ocean Marine Heatwaves Assessed Using a Global Ocean Circulation Model. *Frontiers in Climate*, *4*. doi: 10.3389/fclim.2022.788390

Masson-Delmotte, V., P. Z., A. Pirani, S. L. Connors, C. Péan, S. Berger, ... B.

Zhou (eds.) (2021). *IPCC, 2021: Summary for Policymakers. In: Climate Change 2021: The Physical Science Basis. Contribution of Working Group I to the Sixth Assessment Report of the Intergovernmental Panel on Climate Change* (Tech. Rep.).

Maulida, T., Wirasatriya, A., Ismunarti, D. H., & Puryajati, A. D. (2022). Physical drivers of the 2013 marine heatwave in the seas of the southern Java-Nusa Tenggera. *Geographia Technica*, *17*, 129–139. doi: 10.21163/GT_2022.171.10

McAdam, R., Masina, S., & Gualdi, S. (2022). Seasonal forecasting of subsurface marine heat waves. *Submitted to Nature Communications*(2023), 1–11. doi: 10.1038/s43247-023-00892-5

Moore, J. K., Doney, S. C., & Lindsay, K. (2004). Upper ocean ecosystem dynamics and iron cycling in a global three-dimensional model. *Global Biogeochemical Cycles*, *18*(4), 1–21. doi: 10.1029/2004GB002220

Moore, J. K., Lindsay, K., Doney, S. C., Long, M. C., & Misumi, K. (2013). Marine ecosystem dynamics and biogeochemical cycling in the community earth system model [CESM1(BGC)]: Comparison of the 1990s with the 2090s under the RCP4.5 and RCP8.5 scenarios. *Journal of Climate*, *26*(23), 9291–9312. doi: 10.1175/JCLI-D-12-00566.1

Morrison, A. K., Frölicher, T. L., & Sarmiento, J. L. (2015). Upwelling in the Southern Ocean. *Physics Today*, *68*(1), 27–32. doi: 10.1063/PT.3.2654

Nam, S., Kim, H. J., & Send, U. (2011). Amplification of hypoxic and acidic events by la Niña conditions on the continental shelf off California. *Geophysical Research Letters*, *38*(22), 1–5. doi: 10.1029/2011GL049549

Negrete-García, G., Lovenduski, N. S., Hauri, C., Krumhardt, K. M., & Lauvset, S. K. (2019). Sudden emergence of a shallow aragonite saturation horizon in the Southern Ocean. *Nature Climate Change*, *9*(4), 313–317. doi: 10.1038/s41558-019-0418-8

Oliver, E. C., Benthuysen, J. A., Darmaraki, S., Donat, M. G., Hobday, A. J., Holbrook, N. J., ... Gupta, A. S. (2021). Marine Heatwaves. *Annual Review of Marine Science*, *13*(1), 1–30. doi: 10.1146/annurev-marine-032720-095144

Oliver, E. C., Donat, M. G., Burrows, M. T., Moore, P. J., Smale, D. A., Alexander, L. V., ... Wernberg, T. (2018). Longer and more frequent marine heatwaves over the past century. *Nature Communications*, *9*(1), 1–12. doi: 10.1038/s41467-018-03732-9

Orr, J. C., Fabry, V. J., Aumont, O., Bopp, L., Doney, S. C., Feely, R. A., ... Yool, A. (2005). Anthropogenic ocean acidification over the twenty-first century and its impact on calcifying organisms. *Nature*, *437*, 681–686. doi: 10.1038/nature04095

Pan, T. C., Applebaum, S. L., & Manahan, D. T. (2015). Experimental ocean acidification alters the allocation of metabolic energy. *Proceedings of the National Academy of Sciences of the United States of America*, *112*(15), 4696–4701. doi: 10.1073/pnas.1416967112

Paulmier, A., & Ruiz-Pino, D. (2009). Oxygen minimum zones (OMZs) in the modern ocean. *Progress in Oceanography*, *80*(3-4), 113–128. Retrieved from `http://dx.doi.org/10.1016/j.pocean.2008.08.001` doi: 10.1016/j.pocean.2008.08.001

Paulmier, A., Ruiz-Pino, D., & Garçon, V. (2011). CO2 maximum in the oxygen minimum zone (OMZ). *Biogeosciences*, *8*(2), 239–252. doi: 10.5194/bg-8-239-2011

Pellichero, V., Sallée, J.-B., Schmidtko, S., Roquet, F., & Charrassin, J.-B. (2017). The ocean mixed layer under Southern Ocean sea-ice: Seasonal cycle and forcing. *Journal of Geophysical Research: Oceans*, *122*(2), 1608–1633. doi: 10.1002/2016JC011970

Pirotta, E., Thomas, L., Costa, D. P., Hall, A. J., Harris, C. M., Harwood, J., ... Tyack, P. L. (2022). Understanding the combined effects of multiple stres-

sors: A new perspective on a longstanding challenge. *Science of the Total Environment*, *821*, 153322. doi: 10.1016/j.scitotenv.2022.153322

Pörtner, H. O. (2002). Climate variations and the physiological basis of temperature dependent biogeography: Systemic to molecular hierarchy of thermal tolerance in animals. *Comparative Biochemistry and Physiology - A Molecular and Integrative Physiology*, *132*(4), 739–761. doi: 10.1016/S1095-6433(02)00045-4

Pörtner, H. O., & Knust, R. (2007). Climate Change Affects Marine Fishes Through the Oxygen Limitation of Thermal Tolerance. *Science*, *315*, 95–97. doi: 10.1259/0007-1285-53-633-920-b

Qi, R., Zhang, Y., Du, Y., & Feng, M. (2022). Characteristics and Drivers of Marine Heatwaves in the Western Equatorial Indian Ocean. *Journal of Geophysical Research: Oceans*, *127*(10), e2022JC018732. doi: 10.1029/2022JC018732

Ramadhan, A., Marshall, J., Meneghello, G., Illari, L., & Speer, K. (2022). Observations of Upwelling and Downwelling Around Antarctica Mediated by Sea Ice. *Frontiers in Marine Science*, *9*. doi: 10.3389/fmars.2022.864808

Righetti, D., Vogt, M., Gruber, N., Psomas, A., & Zimmermann, N. E. (2019). Global pattern of phytoplankton diversity driven by temperature and environmental variability. *Science Advances*, *5*(5). doi: 10.1126/sciadv.aau6253

Riquelme-Bugueño, R., Pérez-Santos, I., Alegría, N., Vargas, C. A., Urbina, M. A., & Escribano, R. (2020). Diel vertical migration into anoxic and high-pCO2 waters: acoustic and net-based krill observations in the Humboldt Current. *Scientific Reports*, *10*(1), 1–11. doi: 10.1038/s41598-020-73702-z

Ritz, D. A., Hobday, A. J., Montgomery, J. C., & Ward, A. J. W. (2011). Chapter Four - Social Aggregation in the Pelagic Zone with Special Reference to Fish and Invertebrates. In M. Lesser (Ed.), *Advances in Marine Biology* (Vol. 60, pp. 161–227). Academic Press. doi: 10.1016/B978-0-12-385529-9.00004-4

Rose, K., Gutiérrez, D., Breitburg, D., Conley, D., Craig, K., Froehlich, H., ... Prema, D. (2019). Impacts of ocean deoxygenation on fisheries. In *'Laffoley, D. & Baxter, J.M. (eds.) (2019). Ocean deoxygenation: Everyone's problem - Causes, impacts, consequences and solutions.* (pp. 519–544). IUCN, Gland, Switzerland. doi: 10.2305/IUCN.CH.2019.13.en

Rosselló, P., Pascual, A., & Combes, V. (2023). Assessing marine heat waves in the Mediterranean Sea: a comparison of fixed and moving baseline methods. *Frontiers in Marine Science*, *10*, 1168368. doi: 10.3389/fmars.2023.1168368

Roy, C., & Reason, C. (2001). ENSO related modulation of coastal upwelling in the eastern Atlantic. *Progress in Oceanography*, *49*(1-4), 245–255. doi: 10.1016/S0079-6611(01)00025-8

Samuels, T., Rynearson, T. A., & Collins, S. (2021). Surviving Heatwaves: Thermal Experience Predicts Life and Death in a Southern Ocean Diatom. *Frontiers in Marine Science*, *8*. doi: 10.3389/fmars.2021.600343

Santoso, A., Mcphaden, M. J., & Cai, W. (2017). The Defining Characteristics of ENSO Extremes and the Strong 2015/2016 El Niño. *Reviews of Geophysics*, *55*(4), 1079–1129. doi: 10.1002/2017RG000560

Scannell, H. A., Johnson, G. C., Thompson, L., Lyman, J. M., & Riser, S. C. (2020). Subsurface Evolution and Persistence of Marine Heatwaves in the Northeast Pacific. *Geophysical Research Letters*, *47*(23), 1–10. doi: 10.1029/2020GL090548

Schaeffer, A., & Roughan, M. (2017). Subsurface intensification of marine heatwaves off southeastern Australia: The role of stratification and local winds. *Geophysical Research Letters*, *44*(10), 5025–5033. doi: 10.1002/2017GL073714

Seibel, B. A. (2011). Critical oxygen levels and metabolic suppression in oceanic oxygen minimum zones. *Journal of Experimental Biology*, *214*(2), 326–336. doi: 10.1242/jeb.049171

Seibel, B. A., Schneider, J. L., Kaartvedt, S., Wishner, K. F., & Daly, K. L. (2016). Hypoxia Tolerance and Metabolic Suppression in Oxygen Mini-

mum Zone Euphausiids: Implications for Ocean Deoxygenation and Biogeochemical Cycles. *Integrative and Comparative Biology*, *56*(4), 510–523. doi: 10.1093/icb/icw091

Sen Gupta, A. (2023). *Marine heatwaves: definition duel heats up.*

Sen Gupta, A., Thomsen, M., Benthuysen, J. A., Hobday, A. J., Oliver, E., Alexander, L. V., ... Smale, D. A. (2020). Drivers and impacts of the most extreme marine heatwaves events. *Scientific Reports*, *10*(1), 1–15. doi: 10.1038/s41598-020-75445-3

Smale, D. A., Wernberg, T., Oliver, E. C. J., Thomsen, M., Harvey, B. P., Straub, S. C., ... Moore, P. J. (2019). Marine heatwaves threaten global biodiversity and the provision of ecosystem services. *Nature Climate Change*, *9*(4), 306–312. doi: 10.1038/s41558-019-0412-1

Smith, K. E., Burrows, M. T., Hobday, A. J., King, N. G., Moore, P. J., Sen Gupta, A., ... Smale, D. A. (2023). Biological Impacts of Marine Heatwaves. *Annual review of marine science*, *15*, 119–145. doi: 10.1146/annurev-marine-032122-121437

Smith, R., & Gent, P. (2010). *The Parallel Ocean Program (POP) reference manual* (Tech. Rep.). National Center for Atmospheric Research Boulder, Colorado: National Center for Atmospheric Research Boulder, Colorado.

Stabeno, P. J., & Bell, S. W. (2019). Extreme Conditions in the Bering Sea (2017–2018): Record-Breaking Low Sea-Ice Extent. *Geophysical Research Letters*, *46*(15), 8952–8959. doi: 10.1029/2019GL083816

Stuart-Smith, R. D., Bates, A. E., Lefcheck, J. S., Duffy, J. E., Baker, S. C., Thomson, R. J., ... Edgar, G. J. (2013). Integrating abundance and functional traits reveals new global hotspots of fish diversity. *Nature*, *501*(7468), 539–542. doi: 10.1038/nature12529

Susanto, R. D., Gordon, A. L., & Zheng, Q. (2001). Upwelling along the coasts of Java and Sumatra and its relation to ENSO. *Geophysical Research Letters*, *28*(8), 1599–1602. doi: 10.1029/2000GL011844

Tai, T. C., Sumaila, U. R., & Cheung, W. W. (2021). Ocean Acidification Amplifies Multi-Stressor Impacts on Global Marine Invertebrate Fisheries. *Frontiers in Marine Science*, *8*, 1–12. doi: 10.3389/fmars.2021.596644

Tamsitt, V., Drake, H. F., Morrison, A. K., Talley, L. D., Dufour, C. O., Gray, A. R., ... Weijer, W. (2017). Spiraling pathways of global deep waters to the surface of the Southern Ocean. *Nature Communications*, *8*(1), 1–10. doi: 10.1038/s41467-017-00197-0

Turi, G., Alexander, M., Lovenduski, N. S., Capotondi, A., Scott, J., Stock, C., ... Jacox, M. (2018). Response of O_2 and pH to ENSO in the California Current System in a high-resolution global climate model. *Ocean Science*, *14*(1), 69–86. doi: 10.5194/os-14-69-2018

Vogt, L., Burger, F. A., Griffies, S. M., & Frölicher, T. L. (2022). Local Drivers of Marine Heatwaves: A Global Analysis With an Earth System Model. *Frontiers in Climate*, *4*. doi: 10.3389/fclim.2022.847995

Wilson, E. A., Riser, S. C., Campbell, E. C., & Wong, A. P. (2019). Winter upper-ocean stability and ice-ocean feedbacks in the sea ice-covered Southern Ocean. *Journal of Physical Oceanography*, *49*(4), 1099–1117. doi: 10.1175/JPO-D-18-0184.1

Worm, B., & Tittensor, D. P. (2018). *A theory of global biodiversity* (No. 60). Princeton, New Jersey: Princeton University Press.

Xu, K., Huang, R. X., Wang, W., Zhu, C., & Lu, R. (2017). Thermocline fluctuations in the equatorial pacific related to the two types of El Niño events. *Journal of Climate*, *30*(17), 6611–6627. doi: 10.1175/JCLI-D-16-0291.1

Yang, G., Liu, L., Zhao, X., Li, Y., Duan, Y., Liu, B., ... Yu, W. (2019). Impacts of Different Types of ENSO Events on Thermocline Variability in the Southern Tropical Indian Ocean. *Geophysical Research Letters*, *46*(12), 6775–6785. doi:

10.1029/2019GL082818

Yang, S., & Gruber, N. (2016). The anthropogenic perturbation of the marine nitrogen cycle by atmospheric deposition: Nitrogen cycle feedbacks and the 15N Haber-Bosch effect. *Global Biogeochemical Cycles*, *30*(10), 1418–1440. doi: 10.1002/2016GB005421

Zeebe, R. E., & Wolf-Gladrow, D. (2001). *CO2 in seawater : equilibrium, kinetics, isotopes*. Burlington: Elsevier Burlington.

Zhang, Y., Du, Y., Feng, M., & Hu, S. (2021). Long-Lasting Marine Heatwaves Instigated by Ocean Planetary Waves in the Tropical Indian Ocean During 2015–2016 and 2019–2020. *Geophysical Research Letters*, *48*(21), e2021GL095350. doi: 10.1029/2021GL095350

Zscheischler, J., & Seneviratne, S. I. (2017). Dependence of drivers affects risks associated with compound events. *Science Advances*, *3*(6), 1–11. doi: 10.1126/sciadv.1700263

Zuo, H., Balmaseda, M. A., Tietsche, S., Mogensen, K., & Mayer, M. (2019). The ECMWF operational ensemble reanalysis–analysis system for ocean and sea ice: a description of the system and assessment. *Ocean Science*, *15*(3), 779–808. doi: 10.5194/os-15-779-2019

Supporting Information for "Column-Compound Extremes in the Global Ocean"

Contents of this file

1. Text S1 to S4

   (i) Text S1 - Detrending the data for the fixed and moving baselines.

   (ii) Text S2 - Sensitivity cases of minimum vertical threshold of CCXs.

   (iii) Text S3 - K-means clustering of CCX types into regions.

2. Figures S1 to SX

   (i) Figure S1 - Mean absolute percentage error of the quadratic trend of $[H^+]$ at depths of 5m, 145m, and 285m.

   (ii) Figure S2 - Top: Mean absolute percentage error of the quadratic trend of $[H^+]$, at 5 m for the month of January. Bottom: Annual time series of $[H^+]$ and the fitted quadratic trend at selected points within the map.

   (iii) Figure S3-S6 - Sensitivity cases of different column thresholds using mean CCX days per year.

   (iv) Figure S7 - Evaluation of CESM 20 °C isotherm depth, against ORAS5 re-analysis.

   (v) Figure S8 - Key metrics of MHW-LOX events in the global ocean.

Corresponding author: J. Wong, CHN E29, Universitätstrasse 16, 8092 Zürich, Switzerland (joel.wong@usys.ethz.ch)

(vi) Figure S9 - Key metrics of OAX-LOX events in the global ocean.

(vii) Figure S10 - Plots supporting choice of cluster number for k-means clustering.

(viii) Figure S11 - Annual time series of CCX volume fraction divided by clusters.

Additional Supporting Information (Files uploaded separately)

1. Captions for Movie S1

(i) Video of vertical section detected single extremes of the equatorial Pacific during 1998, at a daily resolution.

Text S1 - Detrending the data for the fixed and moving baselines.

The temperature, $[H^+]$, and $[O_2]$ values from the hindcast were detrended to remove the trend due to climate change over time. Due to the steep increase in $[H^+]$ over the hindcast period, a quadratic trend was chosen to represent this increase (Hauri et al., 2021). For the sake of consistency, a quadratic trend was also used to detrend temperature and $[O_2]$ values, even though their rate of increase is closer to a linear trend. In Figures S1 to **??**, we plot the mean absolute percentage error (MAPE) of the fitted quadratic trend in each month, and three depth levels. The maximum MAPE across all grid cells and depths is 28 %. In areas with the highest MAPE, we found that the error was a result of high interannual variability of $[H^+]$ values. We show this in Figure S2, where the quadratic function fits the overarching trend, but the high variability leads to relatively higher error.

The procedure used to detrend the data is as follows. Temperature, $[H^+]$, and $[O_2]$ values from the hindcast were first monthly-averaged in each grid cell. A quadratic trend is then fitted on the variables in each month and grid cell, over 63 (1958-2020) years of the hindcast. The values of the variables were then detrended to the year 1958, using the monthly fitting coefficients of the quadratic trend. Finally, the seasonal threshold with baseline of 1958 was obtained by taking the 95th (5th) percentile of temperature, $[H^+]$, and $[O_2]$ values over an 11-day rolling window. That is, a total of ($63\,\text{years} * 11\,\text{days} = 693$) values are used to determine the threshold for each day of year.

During detection on a fixed baseline, the non-detrended variables are used, against the 1958 baseline calculated earlier. On a moving baseline, the quadratic trend is added to the 1958 baseline threshold for each year, so that the threshold increases (or decreases for O_2) with the year of the hindcast.

Text S2 - Sensitivity cases of minimum vertical threshold of CCXs.

A threshold of at least 50 m out of the 300 m column is chosen as the definition of a column extreme event. This value was chosen such that a significant fraction (at least 16 %) of the column is occupied by extremes under this definition. Using too small a threshold diminishes the biological relevance of the definition. On the other hand, too large a threshold limits the number of detected extreme events in this study. The considerations behind the choice of this threshold is similar to that of percentile thresholds in MHW studies.

Apart of 50 m, we conducted a sensitivity test of using 25 m, 75 m, and 100 m as the column extreme threshold. Under such threshold changes, we expect the number of detected extreme days to decrease (increase) as the threshold increases (decreases). Upon comparing the mean extreme days per year for each case, we found no significant change in the regional distribution of CCXs. In some regions where the threshold is stricter, we no longer detect CCXs when compared to the 50 m case. Some examples of this include central tropical Pacific, and tropical Indian ocean. These comparison plots are presented in Figures S3-S6 of the supporting information.

Text S3 - K-means clustering of CCX types into regions.

The detected CCXs were regionally clustered using k-means clustering as part of the analysis of their drivers. The dimensions used in the clustering are the vertical locations of single grid cell extremes that occurred as part of a CCX, weighted by the intensity index. First, 6 bins of 50 m each are defined for each single extreme type. Over the entire period of the hindcast, the intensity index of each grid cell single extreme is added to these bins. Finally, k-means clustering is performed on these binned counts of intensity index. Double CCXs are clustered on 12 dimensions, while the triple CCX is clustered on 18 dimensions.

To determine the appropriate number of clusters to be used for each extreme type, computed the sum of squares error (SSE), and Silhouette coefficient for $2-6$ clusters. These values are shown in Figure S10 of the supporting information. The number of clusters for each CCX type was chosen by the Elbow method (using the SSE), and maximising the Silhouette coefficient. One exception to the Elbow method is in MHW-OAX-LOW extremes, where 5 clusters were chosen over 4 , since the SSE decreased while the Silhouette coefficient increased.

Video of vertical section of the equatorial Pacific during years 1997-1999.

References

Hauri, C., Pagès, R., McDonnell, A. M., Stuecker, M. F., Danielson, S. L., Hedstrom, K., ... Doney, S. C. (2021). Modulation of ocean acidification by decadal climate variability in the Gulf of Alaska. *Communications Earth and Environment*, *2*(1), 1–7. Retrieved from `http://dx.doi.org/10.1038/s43247-021-00254-z` doi: 10.1038/s43247-021-00254-z

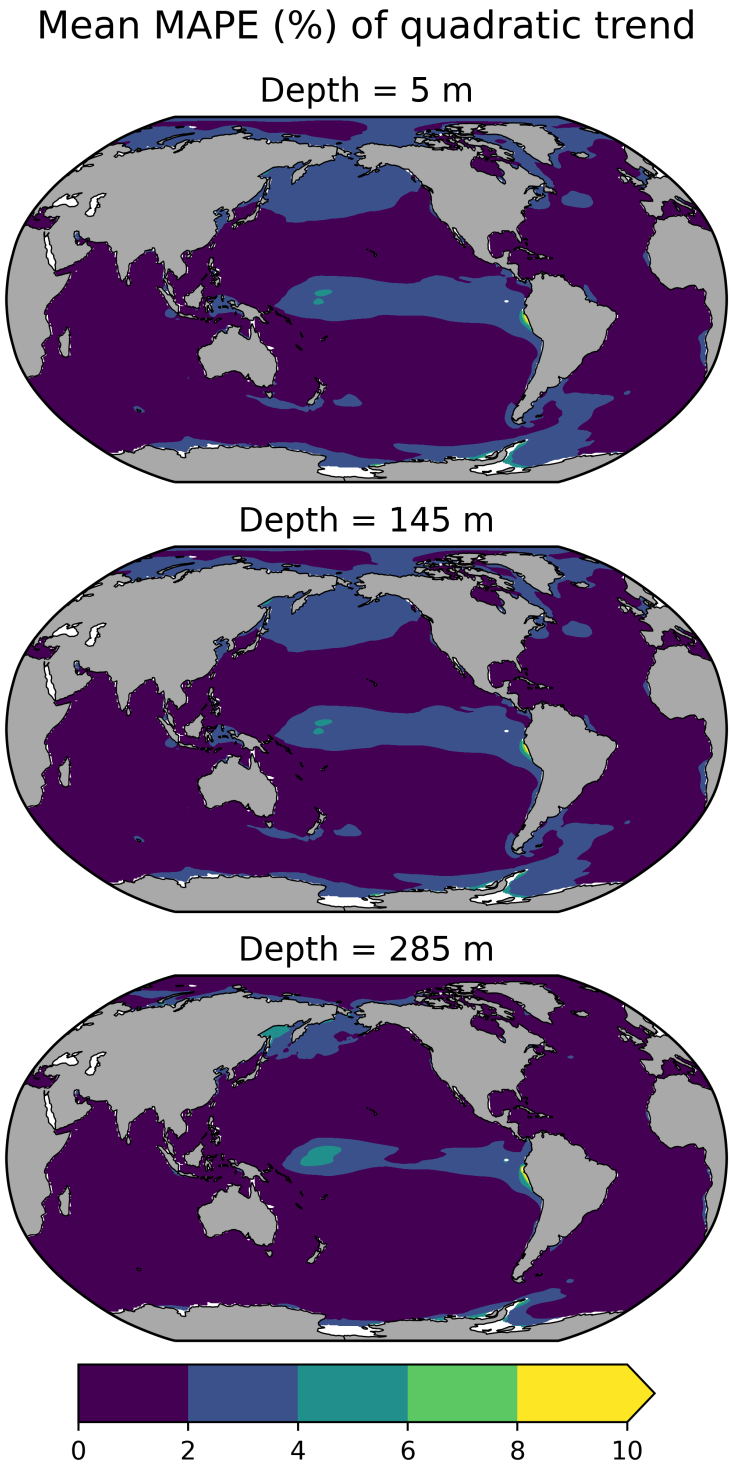

Figure S1. Mean absolute percentage error of the quadratic trend of $[H^+]$ at depths of 5m, 145m, and 285m.

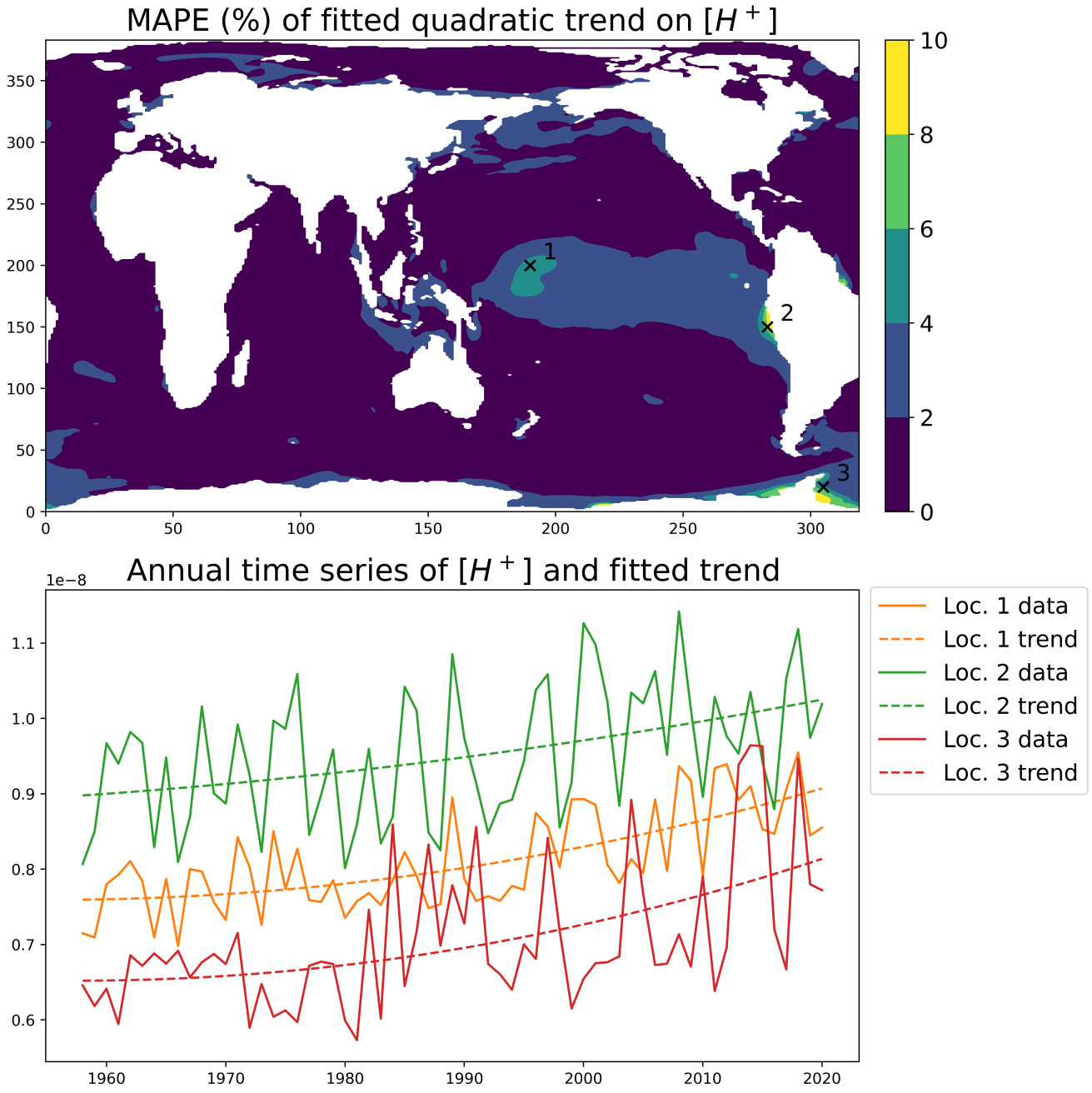

Figure S2. Top: Mean absolute percentage error of the quadratic trend of $[H^+]$, at 5 m for the month of January. Bottom: Annual time series of $[H^+]$ and the fitted quadratic trend at selected points within the map.

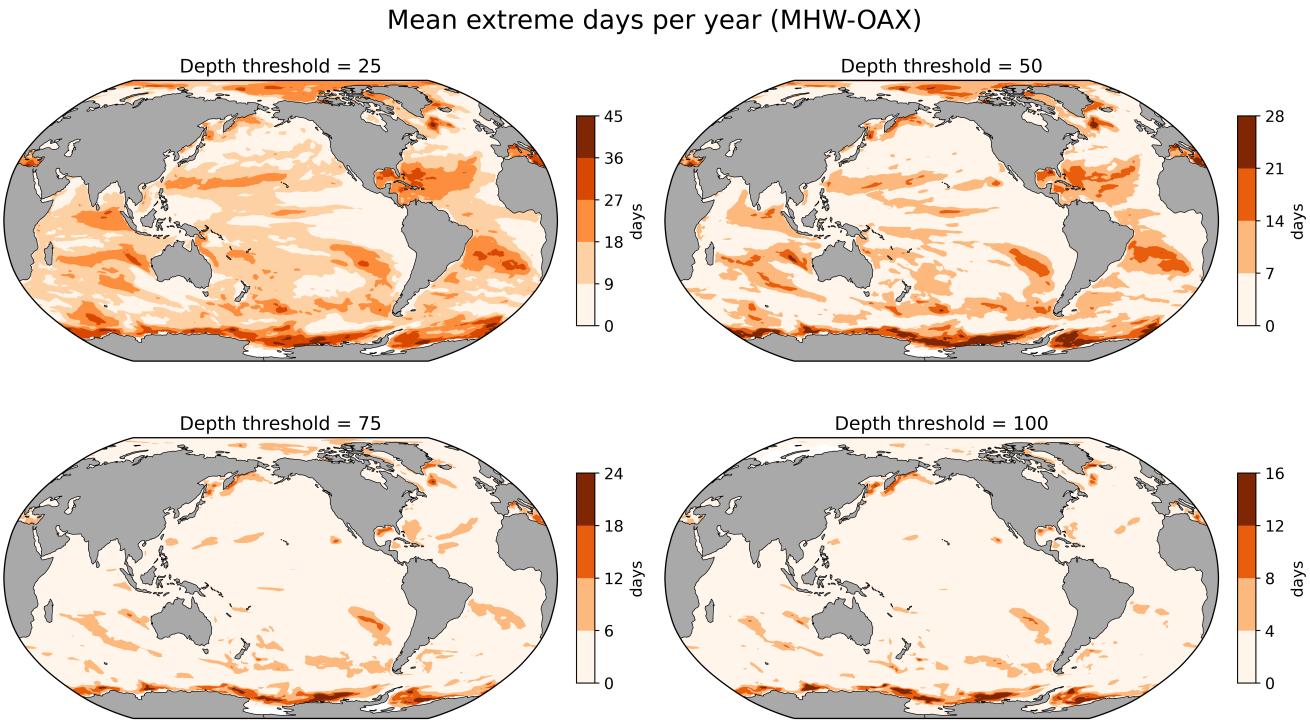

Figure S3. Sensitivity cases of different column thresholds on the mean CCX days per year of MHW-OAX.

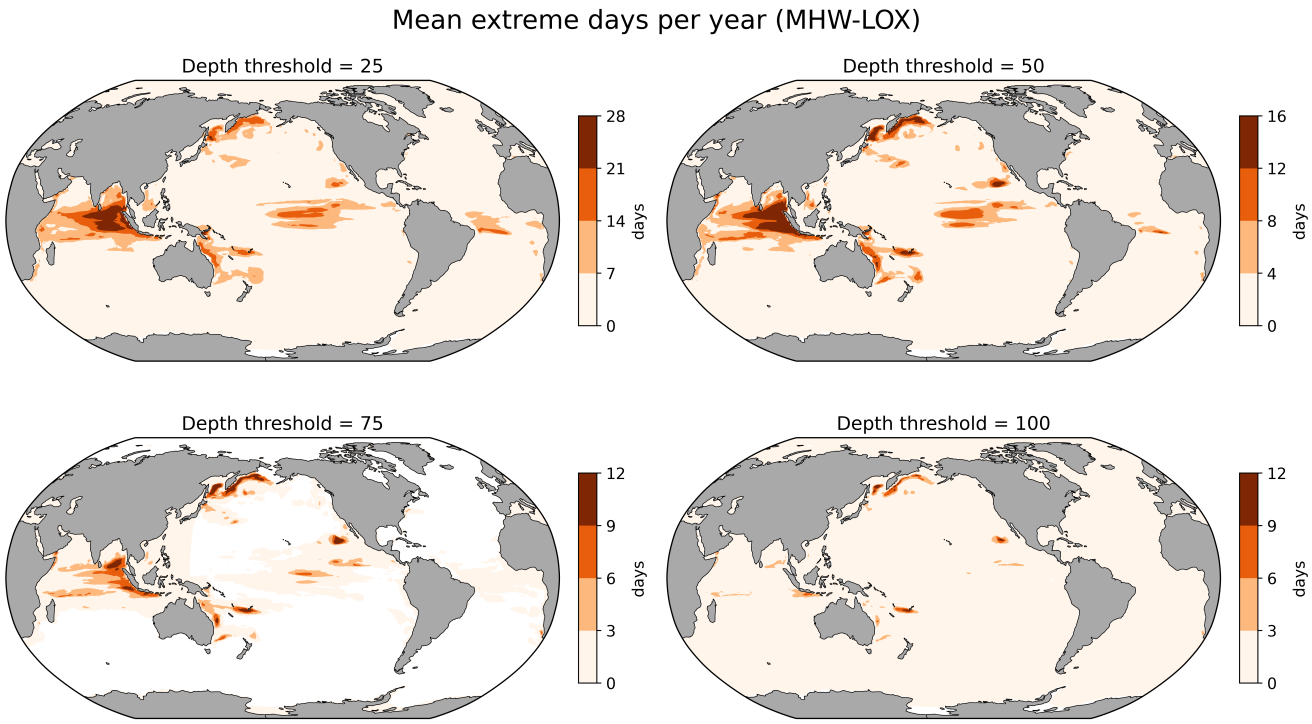

Figure S4. Sensitivity cases of different column thresholds on the mean CCX days per year of MHW-LOX.

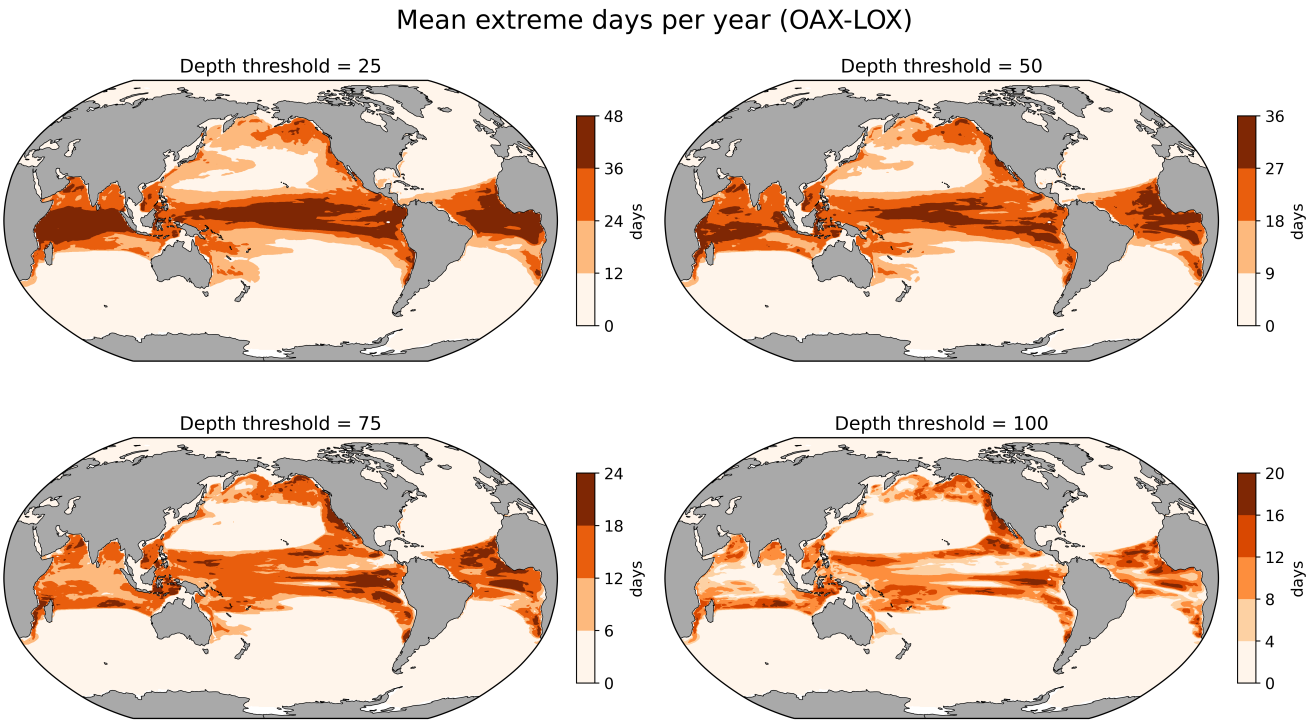

Figure S5. Sensitivity cases of different column thresholds on the mean CCX days per year of OAX-LOX.

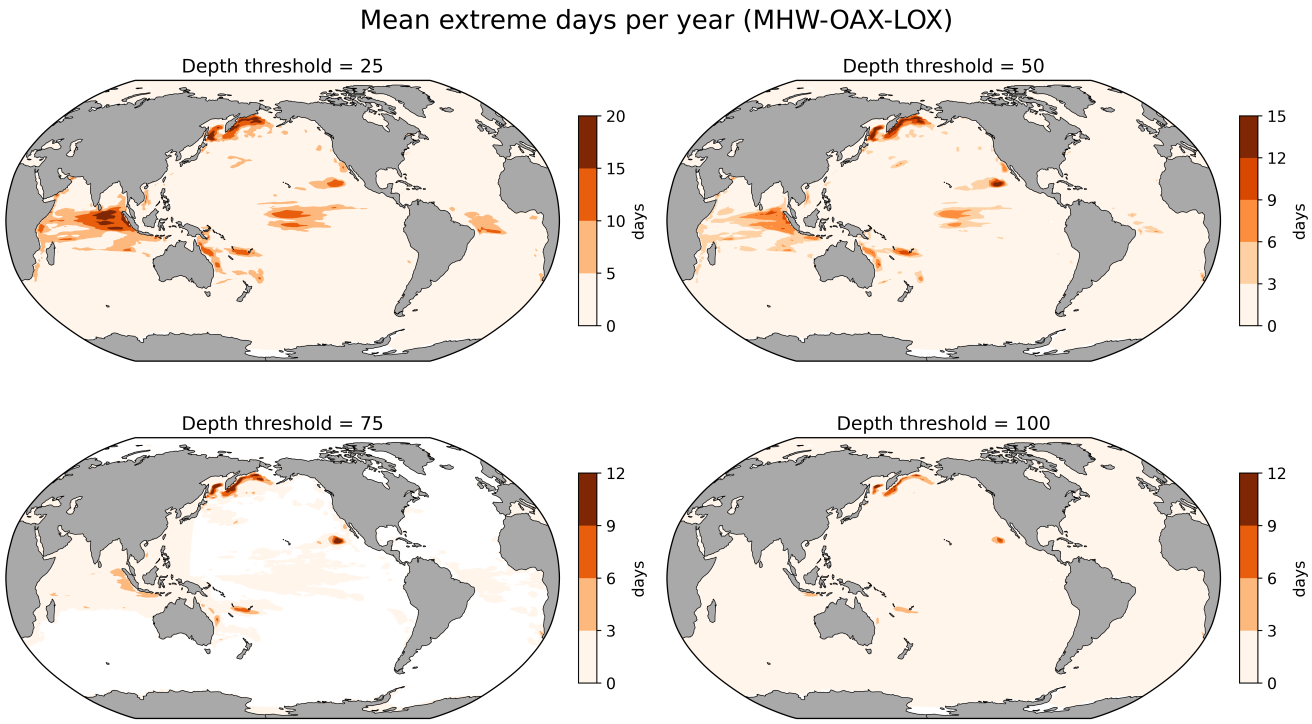

Figure S6. Sensitivity cases of different column thresholds on the mean CCX days per year of MHW-OAX-LOX.

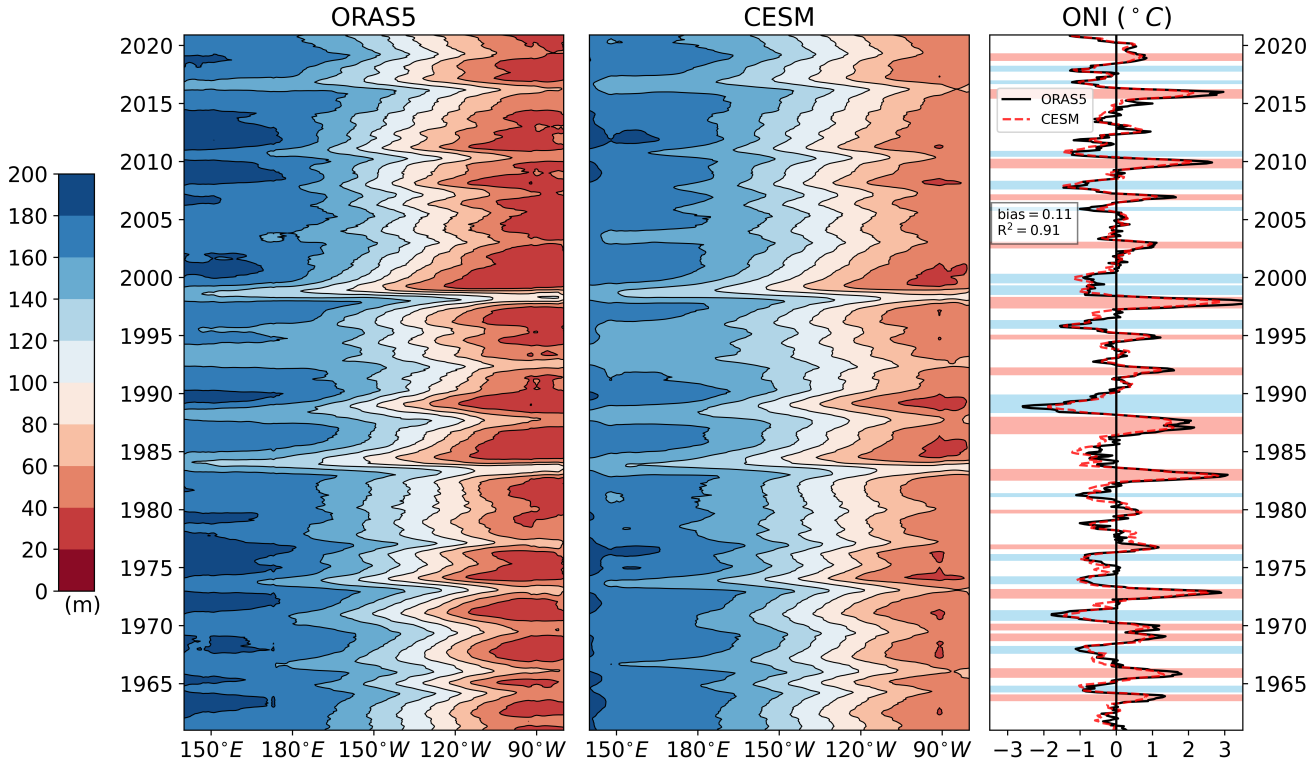

Figure S7. Evaluation of CESM 20 °C isotherm depth, against ORAS5 re-analysis. A time-series of ONI from CESM (black dotted) and ORAS5 (red solid) is shown on the right, where El Niño periods are shaded in red, and La Niña in blue.

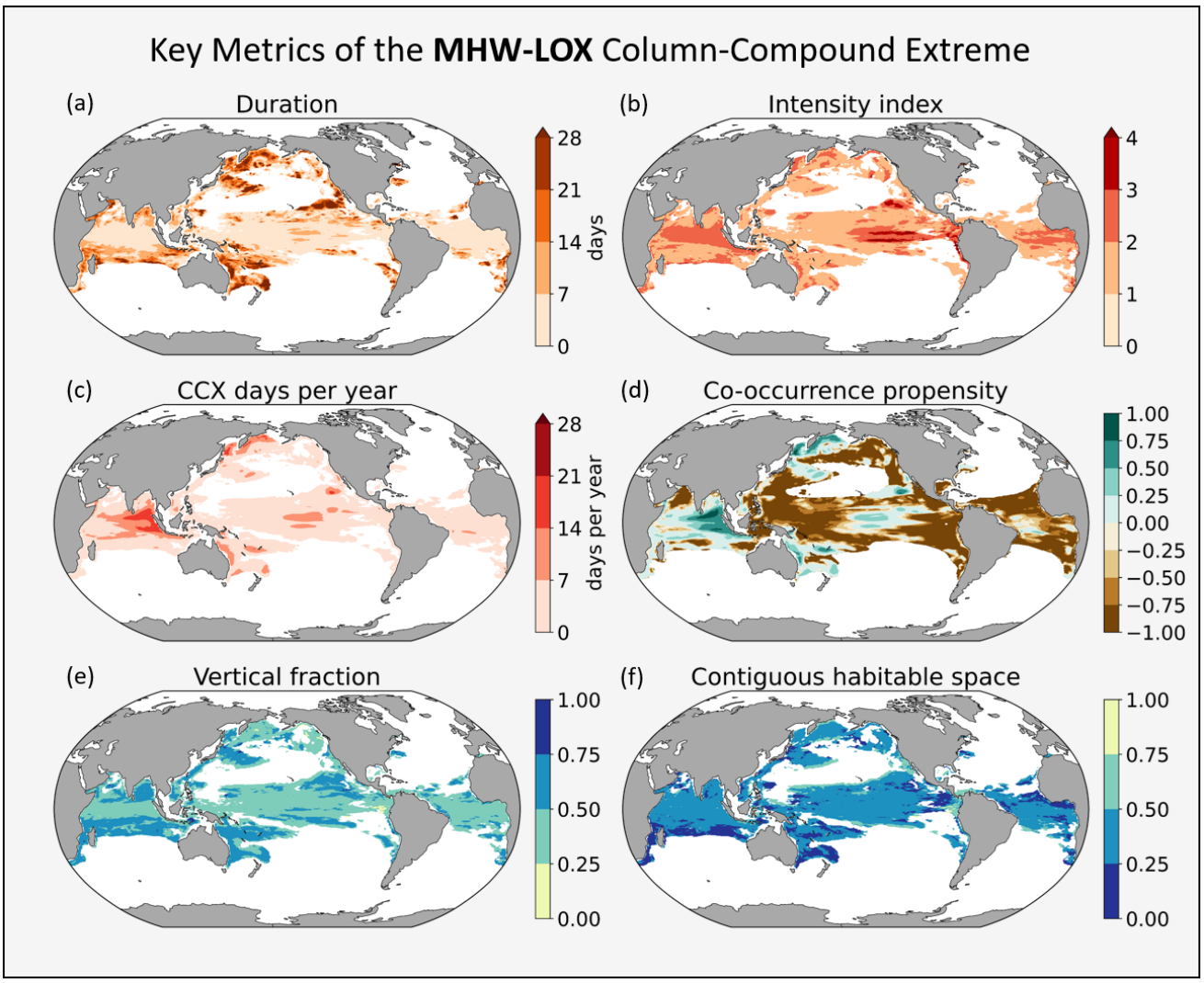

Figure S8. Key metrics of MHW-LOX events in the global ocean. (a) Mean duration, (b) mean annual maximum intensity index, (c) mean days per year, (d) mean co-occurrence propensity, (e) mean fraction of water column occupied by extremes, and (f) mean fraction of contiguous habitable space in the vertical column

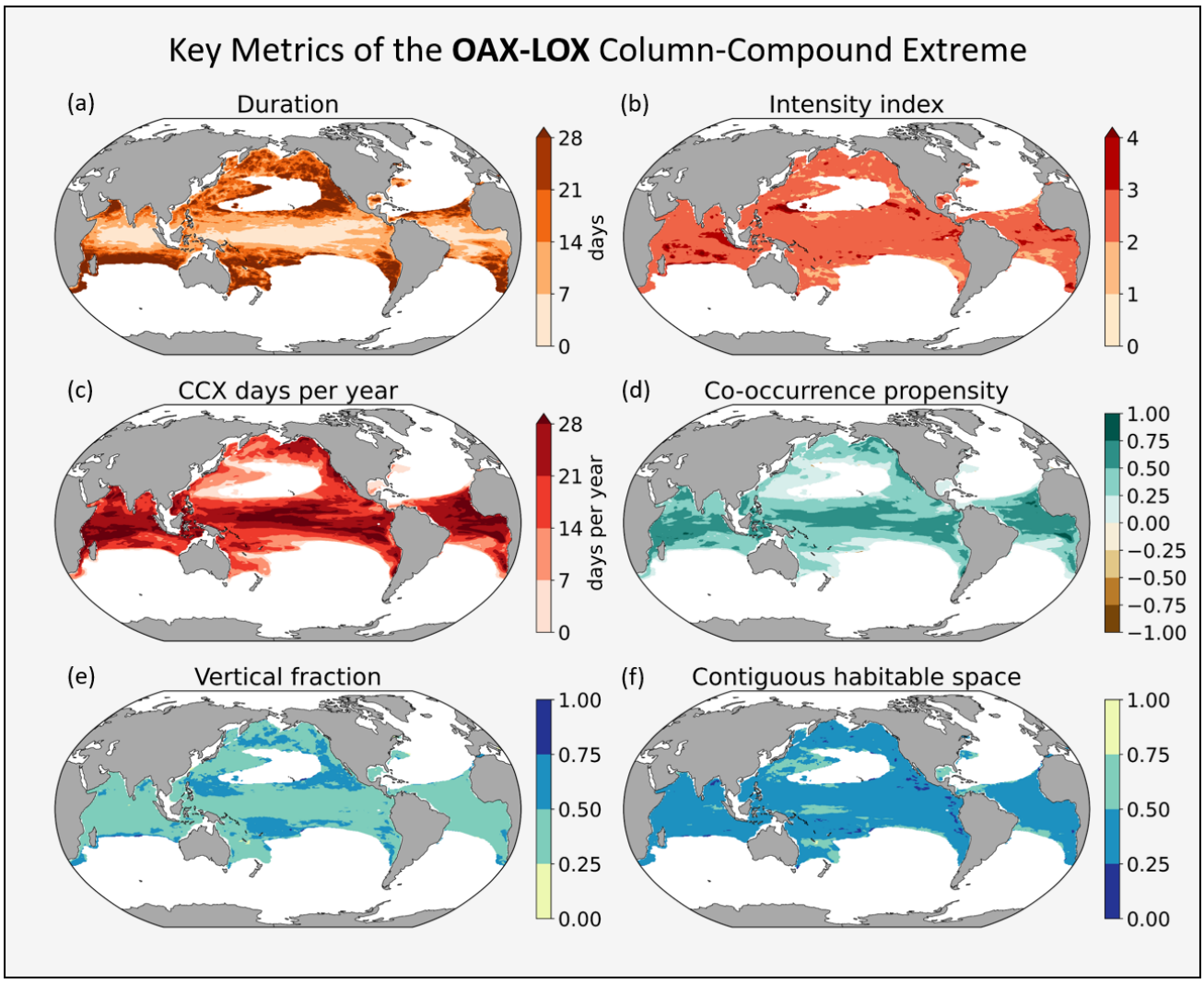

Figure S9. Key metrics of OAX-LOX events in the global ocean. (a) Mean duration, (b) mean annual maximum intensity index, (c) mean days per year, (d) mean co-occurrence propensity, (e) mean fraction of water column occupied by extremes, and (f) mean fraction of contiguous habitable space in the vertical column

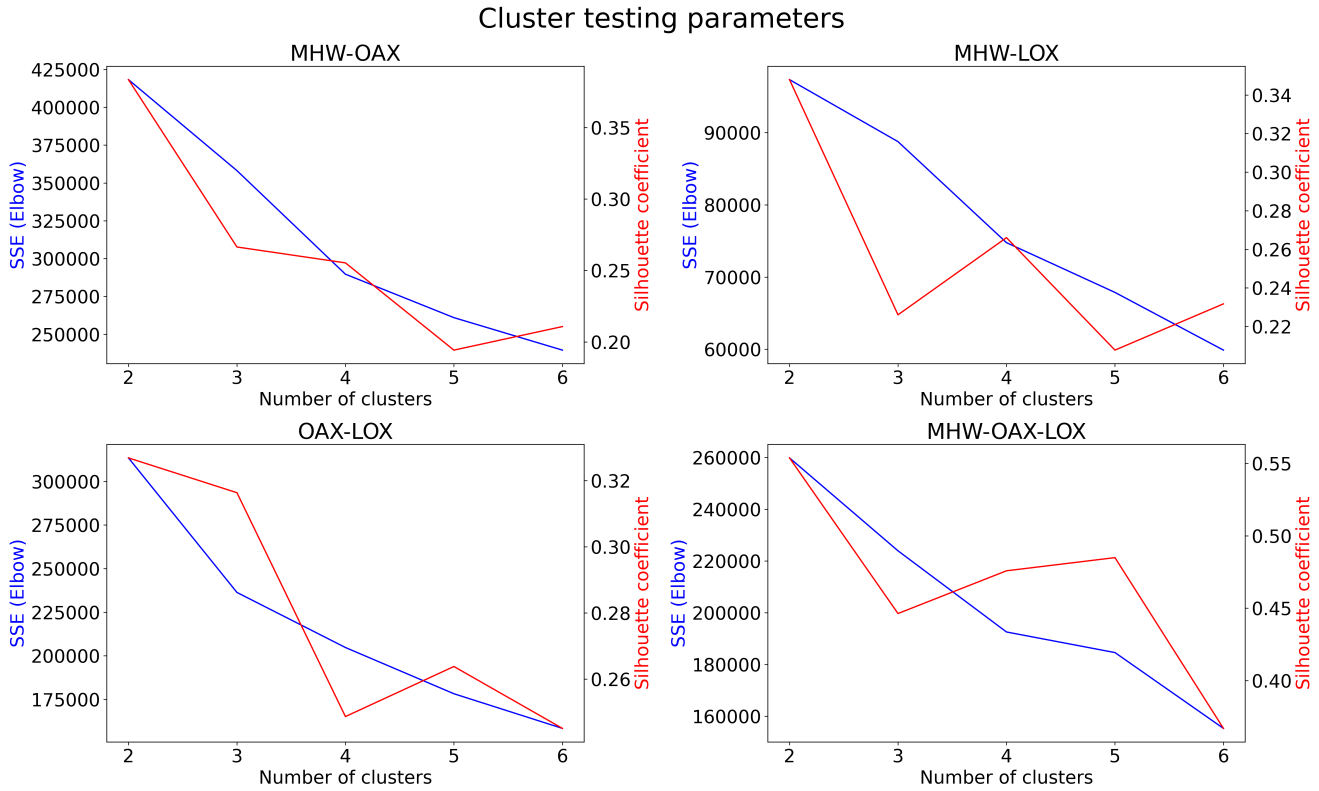

Figure S10. Sum of square errors (SSE) and Silhouette coefficient for 2-6 clusters for each type of CCX.

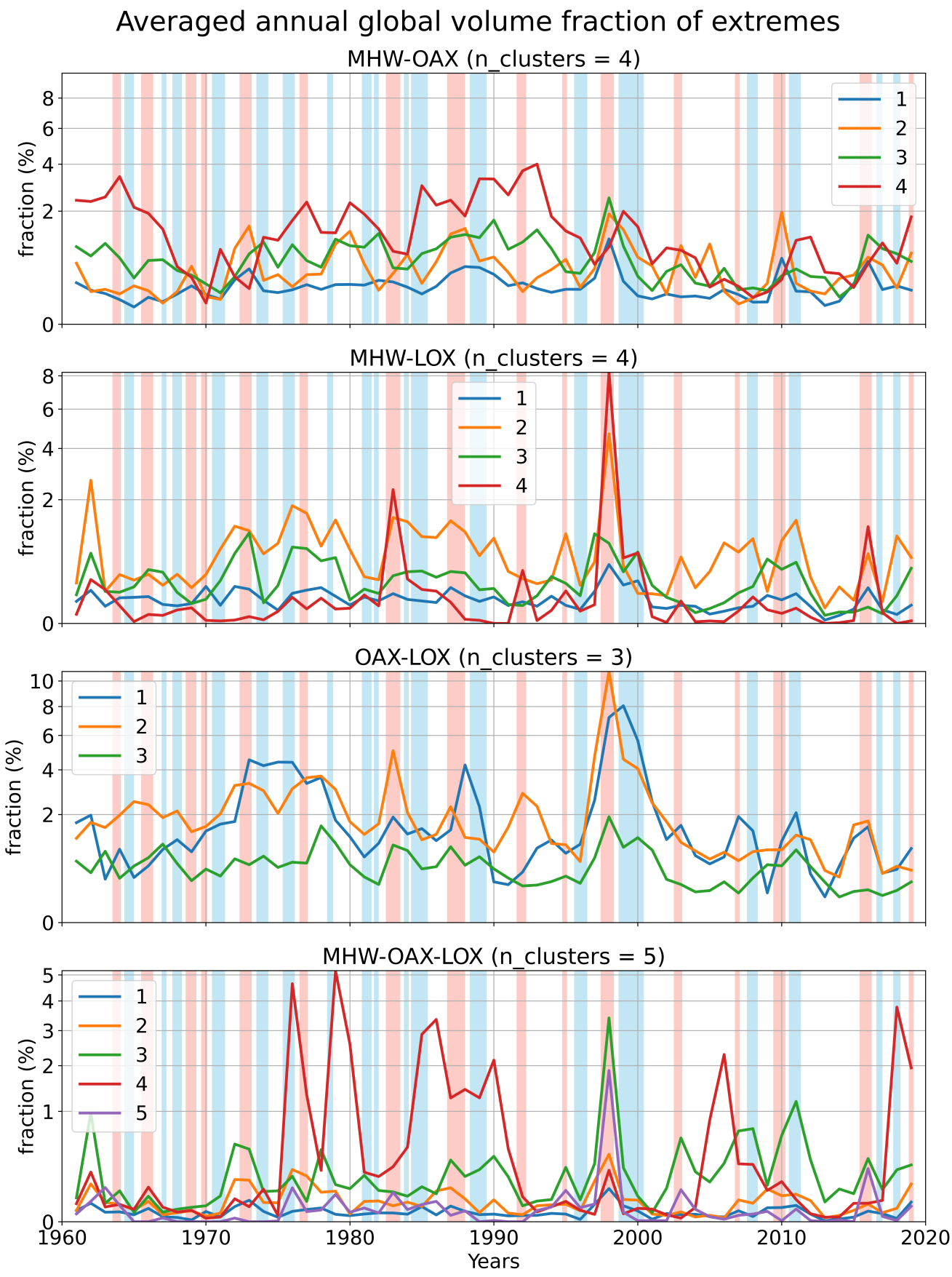

Figure S11. Annual time series of CCX volume fraction divided by clusters.